Received January 29, 2022, accepted February 25, 2022, date of publication March 2, 2022, date of current version March 10, 2022.

Digital Object Identifier 10.1109/ACCESS.2022.3155764

Interplay Between γ–Ray Irradiation and 3DEG for Dosimeter Applications

KHUSHWANT SEHRA[1], (Graduate Student Member, IEEE), VANDANA KUMARI[2], (Member, IEEE), POONAM KASTURI[3], (Member, IEEE), MRIDULA GUPTA[1], (Senior Member, IEEE), MEENA MISHRA[4], (Member, IEEE), DIPENDRA SINGH RAWAL[4], (Member, IEEE), AND MANOJ SAXENA[3], (Senior Member, IEEE)

[1]Department of Electronic Science, University of Delhi South Campus, New Delhi 110021, India
[2]Department of Electronics, Maharaja Agrasen College, University of Delhi, New Delhi 110096, India
[3]Department of Electronics, Deen Dayal Upadhyaya College, University of Delhi, New Delhi 110078, India
[4]Solid State Physics Laboratory, Defence Research and Development Organization, New Delhi 110054, India

Corresponding author: Manoj Saxena (saxena_manoj77@yahoo.co.in)

This work was supported in part by the Department of Biotechnology (DBT) Star College Laboratory, Deen Dayal Upadhyaya College, University of Delhi; in part by the Semiconductor Device Research Laboratory (SDRL), Department of Electronic Science, University of Delhi South Campus; in part by the Institution of Eminence (IoE), Delhi University, under Grant IoE/FRP/PCMS/2020/27 and Grant IoE/2021/12/FRP; and in part by the Solid State Physics Laboratory (SSPL) Contract for Acquisition of Research Services (CARS) Project by the Defence Research and Development Organization (DRDO) under Grant 1115/CARS-73/TS/SPL/18.

ABSTRACT This work investigates the cumulative dose ^{60}Co gamma (γ) – ray irradiation effects on enhancement mode HEMT devices inheriting 3D – Electron and Hole Gases for dosimeter applications. The devices are irradiated through a ^{60}Co source and demonstrate the enhancement in the drain current metrics. To elucidate, the said devices were irradiated through different mechanisms and the Compton effect was investigated through contour plots via TCAD simulations. The degradation of Schottky Gate contact and insulator charging affects the 2D – Hole Gas at the GaN cap and thereby affects the bottleneck at the 3DEG sheet. This significantly affects the OFF – state leakage components of the said device and can therefore be exploited for potential use in sensing and dosimeter applications. The leakage components can be exploited further to improve the linearity of the dosimeter by considering different grading profiles of the AlGaN layer. In this regard, a workflow for optimizing the sensitivity and linearity of the dosimeter through different graded profiles is also presented. Amongst all, gaussian graded profiles have been identified as the best – case scenario considering the sensitivity and exhibiting a linear operation.

INDEX TERMS HEMT, enhancement mode, dosimeter, total ionizing dose, compton effect, gamma radiation.

I. INTRODUCTION

Gallium Nitride (GaN) based devices have established themselves as the viable solution for fulfilling the needs of various space and research agencies. It has replaced Silicon, which has reached its theoretical limits, for being the dominating material for various space applications [1]–[5]. The exciting intrinsic properties of GaN, such as the wider direct band – gap, higher breakdown fields, and higher saturation velocity, enable compatibility of such devices for high power and RF applications [6]. Due to the inherent polar nature of the GaN crystal, AlGaN/GaN heterostructures support a 2 – Dimensional Electron Gas (2DEG) channel supported by the spontaneous and piezoelectric polarizations. Ibbetson *et al.* [7] reported that there is a contribution from the surface like donor states as well that maintains charge neutrality with respect to the 2DEG. The electron carriers in the 2DEG channel are free to move virtually in a 2D space between Source and Drain electrodes and are tightly confined along the third direction, i.e., along the device depth. It is for this reason, GaN based devices can exhibit higher carrier mobilities in the 2DEG channel and announce their compatibility for high frequency applications [6].

The 3 – Dimensional Electron Gas (3DEG) concept was conceptualized and demonstrated experimentally by Jena *et al.* [8] in 2002. The group demonstrates that by grading the AlGaN layers, the net positive polarization charge localized at the AlGaN/GaN can be spread across the entire

The associate editor coordinating the review of this manuscript and approving it for publication was Giambattista Gruosso.

AlGaN layer. This will subsequently smear the electron charge across the entire AlGaN layer in a 3D space, giving rise to higher conductivity without external doping. The concept was eventually exploited to realize polarization doped field effect transistors (PolFET), which exhibit higher carrier mobilities due to the absence of ionized impurity scattering [9]. Park *et al.* [10] have proposed and demonstrated experimentally a 2D/3D hybrid channel AlGaN/GaN HEMT architecture which exhibits a quasi 3DEG profile. The architecture as proposed exhibits a flatter transconductance (g_m) profile which improves the linearity performance in comparison to the conventional HEMT architectures. Further, the proposed architecture combines the advantages of High Electron Mobility Transistor (HEMTs) and Metal Semiconductor Field Effect Transistor (MESFETs), in realizing a custom transconductance profile that can be tailored for achieving a higher peak transconductance $\left(g_{m(Max)}\right)$ and hence higher device gain, or for achieving a broader transconductance profile. Further, due to the graded nature of the AlGaN layer, the effective barrier height increases that limit the gate leakage current, thereby improving the breakdown characteristics of the device. It is widely known that the electron saturation velocity (ν_{sat}) of the GaN channel decreases with the electron density [11]. The ν_{sat} of the GaN channel therefore, is directly responsible for controlling the transconductance and current gain profiles of a conventional HEMT [11]. Accordingly, the linearity performance of such architectures gets degraded. This eventually translates into a higher intermodulation distortion through an increased contribution from the higher order harmonics. Bajaj *et al.* [11], [12] have demonstrated graded AlGaN channel PolFETs in which spreading the polarization charge across the graded AlGaN layers in a 3D space results in a distributed electron density and renders a constant ν_{sat} as a function of gate bias. This significantly suppresses the higher order harmonics and improves the linearity of the device [13].

A novel enhancement – mode HEMT architecture incorporating back-to-back graded AlGaN layers to exploit the 3D polarization engineering for realizing 3DEG and 3DHG (hole gas) was demonstrated by Luo *et al.* [14]. This is in contrast to the standard enhancement – mode HEMTs realized through doped GaN cap layers [15]–[18] that suffer from threshold voltage instabilities. The group reports a significant enhancement in the drain current metrics in comparison to the conventional counterpart. Further studies on the architecture [19] reveal an enhancement in the OFF – state breakdown characteristics of the proposed architecture by 23 times compared to the conventional architecture, considering similar gate – drain spacings and physical gate lengths. Deng *et al.* [20] further proposed an enhancement to the original stack by incorporating a GaN buffer between the positive and negative graded AlGaN layers. The 3DEG realized by the positive graded AlGaN layer was used as a conduction channel, while the 3DHG realized by the negative graded AlGaN layer was used as a back barrier to further suppress the buffer leakage current.

TABLE 1. Sensitivity analysis of HEMT architectures under γ – Ray irradiation from literature.

Device	Condition	I_{ON} (mA)	I_{OFF} (pA)	V_{TH} (V)	$g_{M(max)}$ (mS/mm)	Ref.
Conventional UCSB [Dose Rate: 0.07 rad/s]	Pristine	No Significant Change	-	-4.847	Negligeable Change (<0.2 %)	[28]
	10 krad		-	-4.847		
	20 krad		-	-4.848		
	40 krad		-	-4.849		
	60 krad		-	-4.850		
	80 krad		-	-4.852		
	100 krad		-	-4.853		
	200 krad		-	-4.857		
Cree HEMT [Dose Rate: 0.07 rad/s]	Pristine	No Significant Change	-	-3.000	Negligeable Change (<2 %)	
	20 krad		-	-3.017		
	60 krad		-	-3.018		
	120 krad		-	-3.019		
	150 krad		-	-3.019		
	180 krad		-	-3.020		
MOSHEMT with SiN_x [Dose Rate: 50 rad/s]	Pristine	30.00	2.42e3	-5.413	84.803	[29]
	0.3 Mrad	29.71	2.42e3	-5.438	83.961	
	0.9 Mrad	29.22	2.42e3	-5.488	82.564	
	1.8 Mrad	28.84	2.42e3	-5.513	81.454	
	3.6 Mrad	28.39	2.42e3	-5.564	80.198	
MOSHEMT with HfO_2 [Dose Rate: 50 rad/s]	Pristine	24.00	1.05e2	-4.774	88.100	
	0.3 Mrad	23.98	1.05e2	-4.798	88.015	
	0.9 Mrad	23.88	1.05e2	-4.808	87.651	
	1.8 Mrad	23.71	1.05e2	-4.824	87.045	
	3.6 Mrad	23.45	1.05e2	-4.849	86.103	
MISHEMT [Dose Rate: 3 kGy/hr] Sample 1	Pristine	47.6	-	-10.4	-	[30]
	1 kGy	51.2	-	-11.2	-	
	2 kGy	54.5	-	-11.7	-	
	3 kGy	53.5	-	-11.7	-	
	4 kGy	53.0	-	-11.3	-	
	5 kGy	54.0	-	-11.5	-	
MISHEMT [Dose Rate: 3 kGy/hr] Sample 2	Pristine	46.7	-	-10.2	-	
	1 kGy	51.5	-	-11.2	-	
	3 kGy	52.5	-	-11.2	-	
	5 kGy	52.4	-	-11.3	-	
MISHEMT [Dose Rate: 3 kGy/hr] Sample 3	Pristine	47.3	-	-10.3	-	
	1 kGy	52.0	-	-11.2	-	
	5 kGy	51.5	-	-11.1	-	
	10 kGy	53.0	-	-11.4	-	
MISHEMT [Dose Rate: 3 kGy/hr] Sample 4	Pristine	47.9	-	-9.20	-	
	1 kGy	51.9	-	-10.5	-	
	10 kGy	49.8	-	-10.1	-	
	20 kGy	50.7	-	-10.3	-	
Conventional Fat HEMT [Dose Rate: 3 kGy/hr]	Pristine	99.5/mm	6e6	-3.8	-	[31]
	1 kGy	109/mm	9e4	-3.8	-	
	6 kGy	117/mm	8e4	-3.8	-	
	16 kGy	121/mm	7e4	-3.8	-	
Conventional HEMT [Dose Rate: 3 kGy/hr]	Pristine	810/mm	-	-4.9	-	[32]
	1 kGy	819/mm	-	-4.9	-	
	10 kGy	836/mm	-	-4.9	-	
	30 kGy	854/mm	-	-4.9	-	
	60 kGy	903/mm	-	-4.9	-	

Apart from this, several experimental and theoretical reports suggest the role of the strong bonding nature of III – V binary and ternary nitrides [21]–[24] for the radiation hardness of GaN devices.

Radiation induced defects, including radiation induced traps and stress, may alter the material and electrical properties of AlGaN/GaN heterostructures [21]–[25] and lead

to the departure from the expected results. In this regard, several attempts have been made to assess the reliability of GaN HEMTs in the presence of ionizing radiations for specific applications in nuclear reactors and space. Several studies have also reported the sensitivity of GaN HEMT devices towards the ionizing X – Rays [26]–[28] and γ – Rays [28]–[32]. The impact of γ – Rays irradiation on reported HEMT architectures is compiled in Table 1 [28]–[32].

The impact of ionizing radiation as observed from Table 1 (γ – Rays) on conventional HEMT architecture, having a Schottky Metal – Semiconductor (MS) Gate contact, is negligible as far as the change in peak transconductance $\left(g_{m(Max)}\right)$ and pinch – off voltage (V_{TH}) is considered. The ON – State Current (I_{ON}) however, show significant enhancement with γ – Rays dose compared to X – Ray irradiation [26]–[28]. The MOSHEMT architectures, on the other hand, demonstrate a significant shift in the V_{TH} which is enhanced primarily due to the charging of the insulator at MOS/MIS Gate contact. The OFF – state current (I_{OFF}) for both X – Ray [26]–[28] and γ – Ray [28]–[32] irradiation as reported show significant degradation, which causes a major concern regarding the reliability issues of such devices for prolonged use.

A close observation into the cases compiled in Table 1 calls for a principal requirement for detecting ionizing radiations at a low and high dose to avoid the system failure due to a drift in the operating conditions [33]–[35]. There have been attempts made to utilize GaN HEMTs as a comparator to detect ionizing radiations [36], thin film GaN HEMTs for the detection of X – Rays [37], ultrahigh gain AlGaN/GaN HEMTs for the detection of X – Rays and Protons [38], [39], or an attempt to utilize intrinsic properties of GaN to realize Schottky diodes for the detection of α – Particles [40]. However, to the best of the author's knowledge, discrete GaN HEMT devices have not been exploited yet for γ – Ray based dosimeter applications.

This work is an attempt to provide solutions for the early detection of γ – Rays by exploiting the concept of 3DEG inherent in graded AlGaN layers. A detailed study regarding the impact of γ – Rays on the device characteristics and its subsequent optimization for improved sensitivity as a γ – Ray dosimeter is presented in this paper. The contributions of this work are follows:

- The influence of the cumulative dose ^{60}Co gamma (γ) – ray irradiation on the enhancement mode HEMT device incorporating positive and negative graded AlGaN layers has been presented.
- The impact of γ – rays in generating the Compton electrons, and thus the electron hole pairs in the target device is investigated in depth through contour plots via TCAD simulations.
- The interaction of γ – rays with 3DEG and its pronounced effect on depleting the 2DHG has been exploited for the dosimeter applications and hence the impact of sensitivity towards γ – ray dose has also been carried out under different dose rate environments.
- The sensitivity of the dosimeter has been optimized by considering different graded profiles and it is observed that the gaussian graded AlGaN profile demonstrates the best-case scenario for dosimetry considering linearity and sensitivity metrics.

The device architecture investigated for dosimetry and the models adopted for Victory TCAD Simulations [41] is discussed in *Section 2*. Sensitivity analysis and optimization of the device architecture as a function of γ – Ray dose is presented in *Section 3*. Finally, the paper is concluded in *Section 4*.

II. DEVICE ARCHITECTURE AND CALIBRATION

This section of the paper presents a detailed insight into the TCAD workflow for calibrating the device architecture. The calibration has been validated by developing and realizing the devices through process recipe and virtual fabrication process.

A. DEVICE ARCHITECTURE UNDER TEST

A schematic view of the enhancement mode HEMT device incorporating positive and negative graded AlGaN layers is depicted in Fig. 1(a), and the calibrated simulation deck depicting transfer characteristics is shown in Fig. 1(b). The positive and negative graded AlGaN layers are with regards to an increase/decrease in the Aluminum mole fraction (χ_{Al}) with the growth direction of the graded AlGaN layers [20]. The device dimensions are briefly summarized in Table 2.

The device dimensions and the reference data for calibrating the simulation deck in TCAD are as per Deng *et al.* [20]. The device architecture has a trench gate arrangement supported by a 10 nm HfO_2 dielectric layer, exhibiting a physical gate length (L_G) of 0.5 μm. Starting with the Sapphire Substrate, the epi layer stack of the DUT consists of a 500 nm negative graded AlGaN layer which is supported by a 100 nm AlN nucleation layer. The negative gradient of χ_{Al} spreads the net negative polarization charge in a 3D space, which is screened by the development of a 3DHG acting as a back barrier. The back barrier helps to limit the gate leakage current and consequently improves the OFF – state breakdown characteristics. A 100 nm positive graded AlGaN layer supported by a 700 nm GaN buffer on top of the negative graded AlGaN layer is subsequently grown. The positive gradient of χ_{Al} spreads the net positive polarization charge localized at the AlGaN/GaN (Buffer) interface across the entire AlGaN layer in a 3D space, to smear the electron gas and realize a 3DEG sheet for conduction. Finally, the epi stack consists of a 20 nm partially doped GaN top layer which exhibits a 2DHG (hole gas) localized at the GaN (top)/AlGaN layer interface to realize an enhancement mode operation. The device architecture exhibits vertical conduction through the formation of an electron accumulation layer (EAL) [20] at the sidewalls of the trench gate when the gate bias is ramped

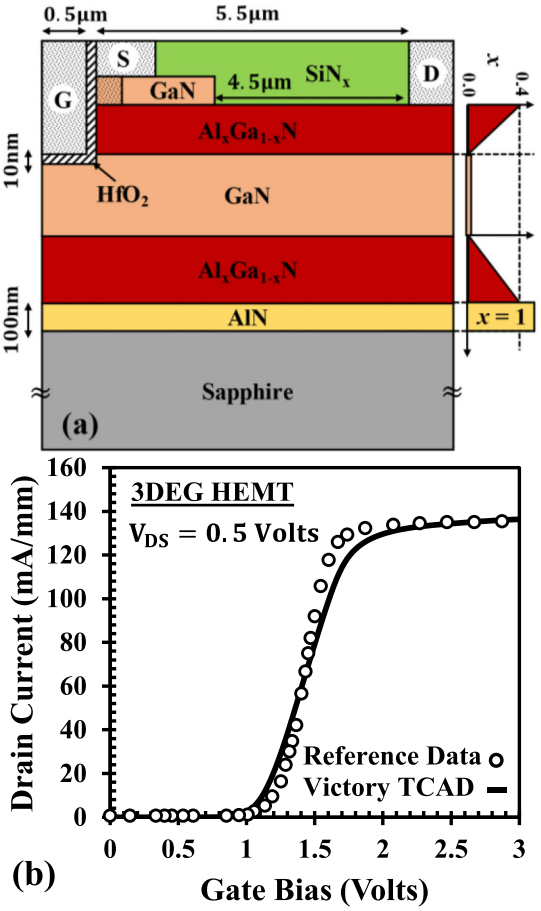

FIGURE 1. (a) Schematic view of the HEMT with 3DEG Conduction Layer and 3DHG as a back barrier, and (b) Calibrated simulation deck depicting transfer characteristics. Reference data is taken from Deng *et al.* [20].

TABLE 2. Device dimensions as in Figure 1.

Symbol	Description	Value
$t_{GaN(top)}$	Thickness of GaN top layer	20 nm
$L_{GaN(top)}$	Length of GaN top layer	1 μm
$N_{GaN(top)}$	Doping of GaN top layer	1×10^{15}cm^{-3}
$N_{s-GaN(top)}$	Highly Doped GaN top layer	1×10^{17}cm^{-3}
$t_{AlGaN(+)}$	Thickness of Positively Graded AlGaN	100 nm
$t_{AlGaN(-)}$	Thickness of Negatively Graded AlGaN	500 nm
t_{GaN}	Thickness of GaN Buffer	700 nm
N_{GaN}	Doping of GaN Buffer	1×10^{15}cm^{-3}
L_G	Gate Length along the Trench	0.5 μm
$L_{G(Actual)}$	Actual Gate Length controlling current flow ($\approx t_{GaN(top)} + t_{AlGaN(+)}$)	120 nm

above the threshold voltage. This, in essence, depletes the 2DHG at GaN (top)/AlGaN layer interface and exhibits an electrical gate length of 120 nm.

B. SIMULATION AND CALIBRATION METHODOLOGY

Silvaco's Victory device simulator tool [41] has been used to carry out the initial calibration of the simulation deck to capture the device's physics and mimic the actual device behavior. Since the device architecture incorporates a partially doped GaN top layer, a Concentration dependent Shockley – Read – Hall (consrh) recombination model was invoked to capture the trap – assisted recombination as a result of trapping states evolved in the partially doped GaN top layer. The carrier statistics are modeled by invoking fermi – dirac statistics (fermi). The degradation in the Gate contact (leading to an increase in OFF – state current) with cumulative γ – Ray dose is captured by invoking the Schottky Tunneling model (ust). The error in the device threshold voltage and the maximum drain current is reduced by tuning the work function of gate contact and the individual spontaneous and piezoelectric polarization components of the AlGaN and GaN layers. Further, since the surface states on AlGaN play a major role in maintaining the charge neutrality with respect to the channel, donor like surface states at the SiN_x/AlGaN and SiN_x/GaN (top) interface were defined with an energy level $E_T = 0.5$ eV, and interface trap density of 3×10^{13}cm^{-2}. The capture cross sections for electrons (σ_n) and holes (σ_p) were set to 1×10^{-13}cm^2. Further, since the bulk traps in GaN buffer are responsible for the degradation in the output admittance parameters [42]–[44], acceptor type traps with $E_T = 0.45$ eV and bulk trap density of 1.5×10^{16}cm^{-3} were defined in GaN buffer with capture cross sections, σ_n and σ_p set to 1×10^{-13}cm^2 respectively. The trapping definitions are in accordance with the experimental studies on similar AlGaN/GaN heterostructures [42]–[44]. Yang *et al.* [45] have also demonstrated through DLTS measurements the evolution of electron and hole traps in doped GaN cap layers, which realize enhancement mode operation. Accordingly, acceptor type traps with $E_T = 0.85$ eV and bulk trap density of 4×10^{16}cm^{-3} with σ_n and σ_p as 1×10^{-15}cm^2 and donor type traps with $E_T = 0.49$ eV, bulk trap density of 3.2×10^{16}cm^{-3} with σ_n and σ_p as 1×10^{-19}cm^2 was defined at the doped GaN top layer in accordance with the DLTS studies [45]. Finally, Albrecht low field mobility model [41] to tune ON – state resistance, and GaNsat high field mobility model [41] to capture the velocity saturation at high fields, were also invoked. In addition to this, to irradiate the DUT with γ – Rays, considering ^{60}Co source, Radiation Effects Module (REM) [41] was invoked in accordance with the methodology presented by Sehra *et al.* [24].

C. PROCESS RECIPE FOR THE VIRTUAL FABRICATION OF DUT

The process recipe for the Virtual Fabrication of DUT through TCAD presented in this section, is an extension of the work reported by Peng *et al.* [19]. Starting with the standard wafer cleansing procedure, the epi layer stack is grown in accordance with the structure depicted in Fig. 1(a) using Metal – Organic Chemical Vapor Deposition (MOCVD) technique on a Sapphire substrate. The active area of the device consists of the positive graded AlGaN layer, which houses the 3DEG channel. The precursors helping in the growth of respective GaN, AlGaN, and AlN layers are the trimethylgallium (TMG - Ga $(CH_3)_3$), trimethylaluminum (TMAl-Al_2 $(CH_3)_6$),

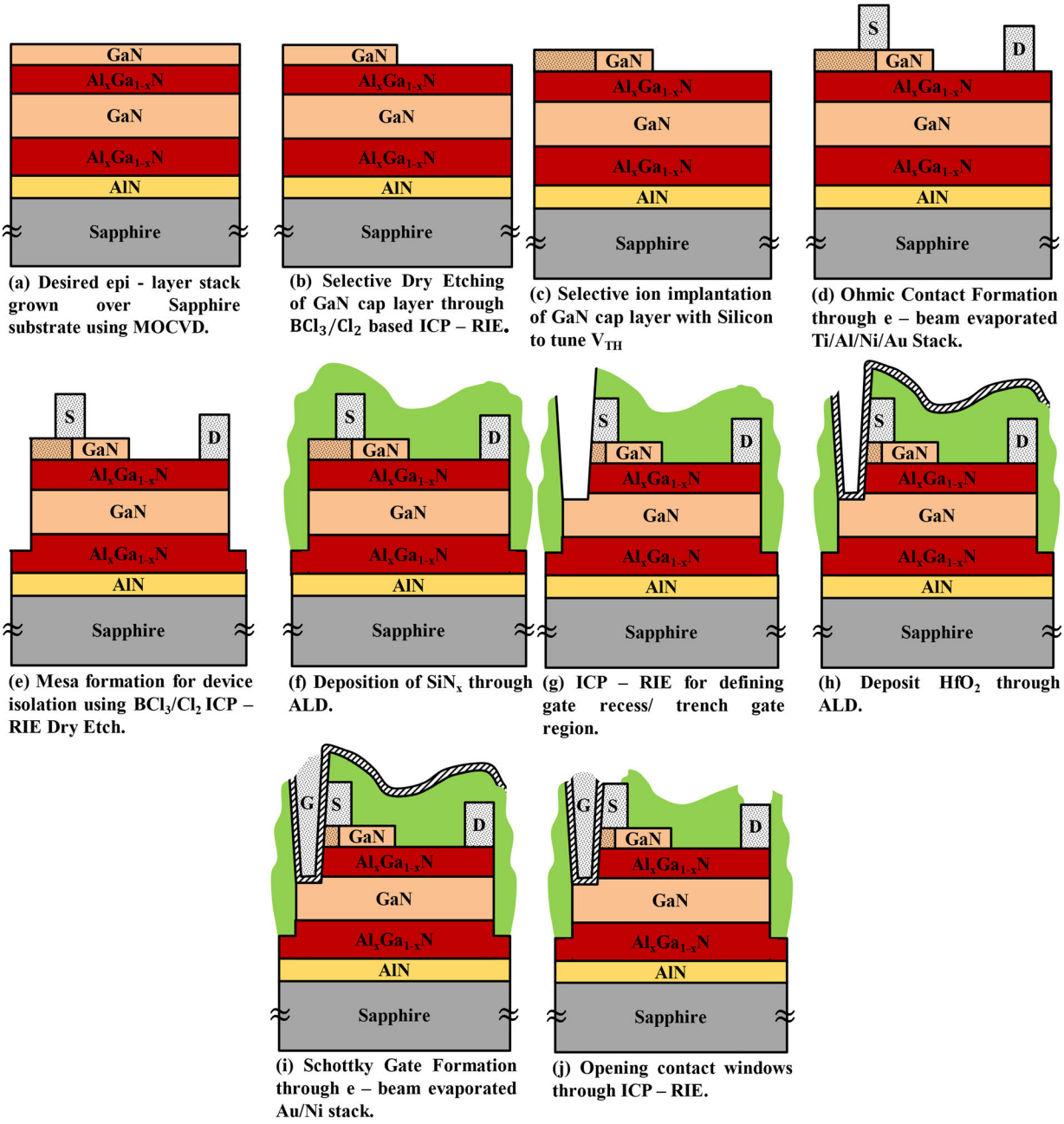

FIGURE 2. Proposed process recipe for the fabrication of HEMT with 3DEG Conduction and 3DHG as back barrier: (a) Desired epi – layer stack grown over Sapphire substrate using MOCVD, (b) Selective Dry Etching of GaN cap layer through BCl_3/Cl_2 based ICP – RIE, (c) Selective ion implantation of GaN cap layer with Silicon to tune V_{TH}, (d) Ohmic Contact Formation through e – beam evaporated Ti/Al/Ni/Au Stack, (e) Mesa formation for device isolation using BCl_3/Cl_2ICP – RIE Dry Etch, (f) Deposition of SiN_x through ALD, (g) ICP – RIE for defining gate recess/ trench gate region, (h) Deposit HfO_2 through ALD, (i) Schottky Gate Formation through e – beam evaporated Au/Ni stack, (j) Opening contact windows through ICP – RIE.

and ammonia (NH_3) with H_2 carrier gas. The χ_{Al} in negative graded AlGaN layer can be controlled by linearly decreasing the TMAl flow to zero, while grading the TMG flow to account for the χ_{Ga} with the growth direction. Similarly, for positive graded AlGaN, the TMAl flow is linearly increased from zero, with the growth direction, while the TMG flow is adjusted to account for the χ_{Ga}. The GaN – top layer is selectively etched towards end point using BCl_3/Cl_2 based ICP – RIE for dry etching. After this appropriate masking is done and selective ion implantation is carried out for doping of GaN – top layer with Silicon to regulate threshold voltage [14], [19], [20]. Standard ohmic contacts are defined using photolithography and e – beam evaporated Ti/Al/Ni/Au stack and standard lift off procedures. The samples are then subjected to rapid thermal processing (RTP) to complete Source and Drain ohmic contact formation.

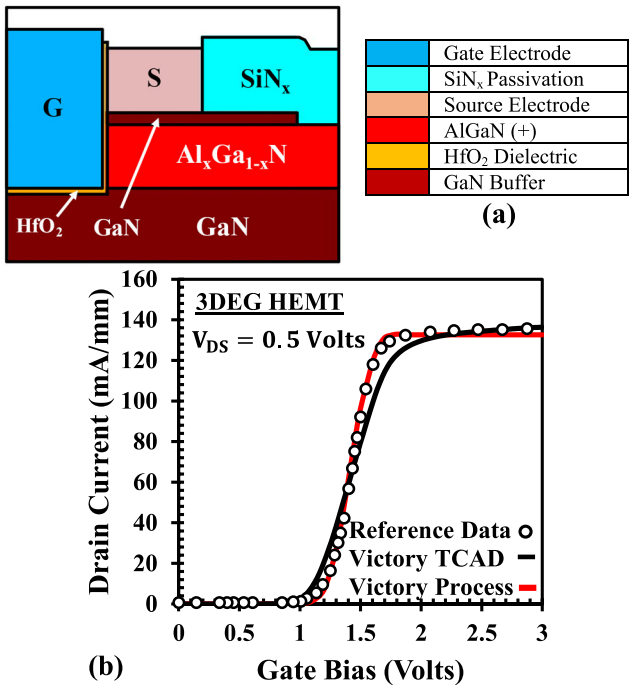

FIGURE 3. (a) Virtual fabrication of the DUT using Silvaco's Victory Process, and (b) Comparison of the resulting transfer characteristics with the TCAD Simulations and Reference data from Deng *et al.* [20].

Post ohmic contact formation, device mesa isolation is carried out through dry etching using BCl_3/Cl_2 based ICP – RIE. This is followed by the deposition of SiN_x passivation layer using Atomic Layer Deposition (ALD) technique. ICP – RIE is then carried out to define the gate trench window. The trench gate formation is then followed up, first by the deposition of HfO_2 through ALD followed by e – beam evaporation of Ni/Au stack for the Gate electrode using standard lift off procedures. Finally, contact windows are opened to get the metal contacts. The process recipe is illustrated in Fig. 2 (i)-(j).

The process steps described above are validated through Silvaco's Victory Process Simulation tools [41] as shown in Fig 3(a) and the transfer characteristics of the virtually fabricated device is shown in Fig. 3(b). The virtually fabricated device is simulated using the trapping parameters given in Section II(B). The proximity of the transfer characteristics with the TCAD analysis validates the process recipe for the fabrication of the DUT.

III. RESULTS AND DISCUSSIONS

The device architecture under study is evaluated for dosimeter applications considering the interaction of γ – Rays from ^{60}Co source with the 3DEG channel housed by the positive graded AlGaN layers. A detailed analysis is presented with regards to the impact on OFF – state and ON – state characteristics of the device with cumulative dose effects of γ – irradiation. Silvaco's Radiation Effects Module (REM) [24], [41] is used to set up a radiation environment from ^{60}Co source with a dose rate of 3 kGy/hr in accordance with the experimental studies [24], [30]–[32].

A. VALIDATION OF RADIATION ENVIRONMENT

To validate the Silvaco's Radiation Effects Module (REM) [24], [41] in capturing the reported experimental effects, the module was initially calibrated against the experimental set reported by Sharma *et al.* [31] at a dose rate of 3 kGy/hr. This calibration is done to capture the experimental γ – ray effects on the AlGaN/GaN material system using the REM module. The calibrated radiation module will be used in the later sections with the calibrated simulation deck of 3DEG HEMTs to assess their sensitivity towards γ – rays. A comparison of the resulting transfer characteristics is shown in Fig. 4(a)-(c) for low and high dose γ – rays. The close proximity of the TCAD data with the experimentally irradiated devices validates the formulations of the Radiation Environment thus set up to test the 3DEG HEMTs for dosimeter applications.

B. IMPACT ON DC CHARACTERISTICS

A comparison of the resulting transfer characteristics under pristine and subsequent γ – Ray irradiation stage is depicted in Fig. 5(a) and enlarged view of the drain current is shown in Fig. 5(b). The resulting effect of γ – Ray on the transconductance profile is shown in Fig. 5(c) with the enlarged view in Fig. 5(d). The impact of γ – Ray irradiation on the shift of device threshold voltage is also summarized in Fig. 5(e). The threshold voltage (V_{TH}) of the pristine device is 0.96 Volt, recorded at 1 mA/mm. A general observation from Fig. 5 (a) and (b) reveals an increase in both the ON – State and OFF – State currents after cumulative γ – Ray irradiations. The increase in ON – State current, recorded for the first dose is greater and then proceeds towards saturation as the devices are irradiated at a higher dose. The Compton effect as a result of interaction of γ – Rays with the electrons, puts the charged carriers into motion (Compton electrons) which eventually results in the generation of electron – hole pairs (EHP). The electron – hole pairs so generated, under the influence of electric field set up in the device, interact with the radiation induced traps and in essence, alter the trapping states already evolved in the epi – layers during fabrication. This eventually leads to a charge buildup in the device as depicted in Fig. 6 (a) and (b) for ON condition and Fig. 6(c) and (d) under OFF state for pristine condition and radiated state. The charge buildup disrupts the charge balance of the 3DEG channel with 2DHG at GaN top layer, which is responsible for creating a bottleneck towards the flow of carriers and helps in realizing an enhancement mode operation. This disruptive effect on 2DHG is exploited in this work to realize a fairly linear response for dosimeter applications.

The principal effect of the interaction of γ – Rays with the GaN HEMTs reported in the literature is the enhancement in sheet carrier density which is coupled to the negative shift in the device threshold voltage ($-\Delta V_{th}$) [23], [28]–[32], [46]. The enhancement in drain current has also been linked with the improvement of carrier mobilities [32], [47]. This improvement, in turn, can be an effect from the relaxation of

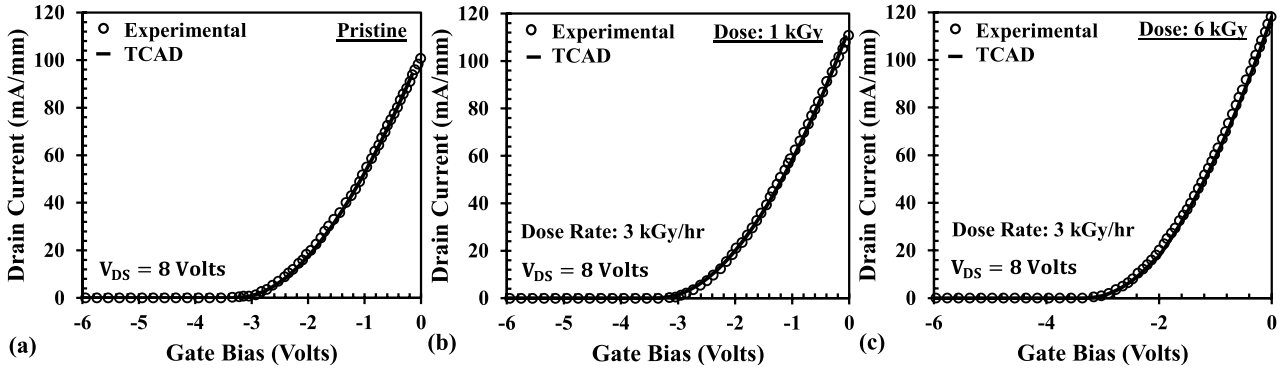

FIGURE 4. Calibration of transfer characteristics of Conventional AlGaN/GaN HEMT under (a) Pristine conditions, and after irradiation at (b) 1 kGy, and (c) 6 kGy with a Dose Rate of 3 kGy/hr. Experimental data from Sharma et. al. [31] is used only for calibrating the radiation module.

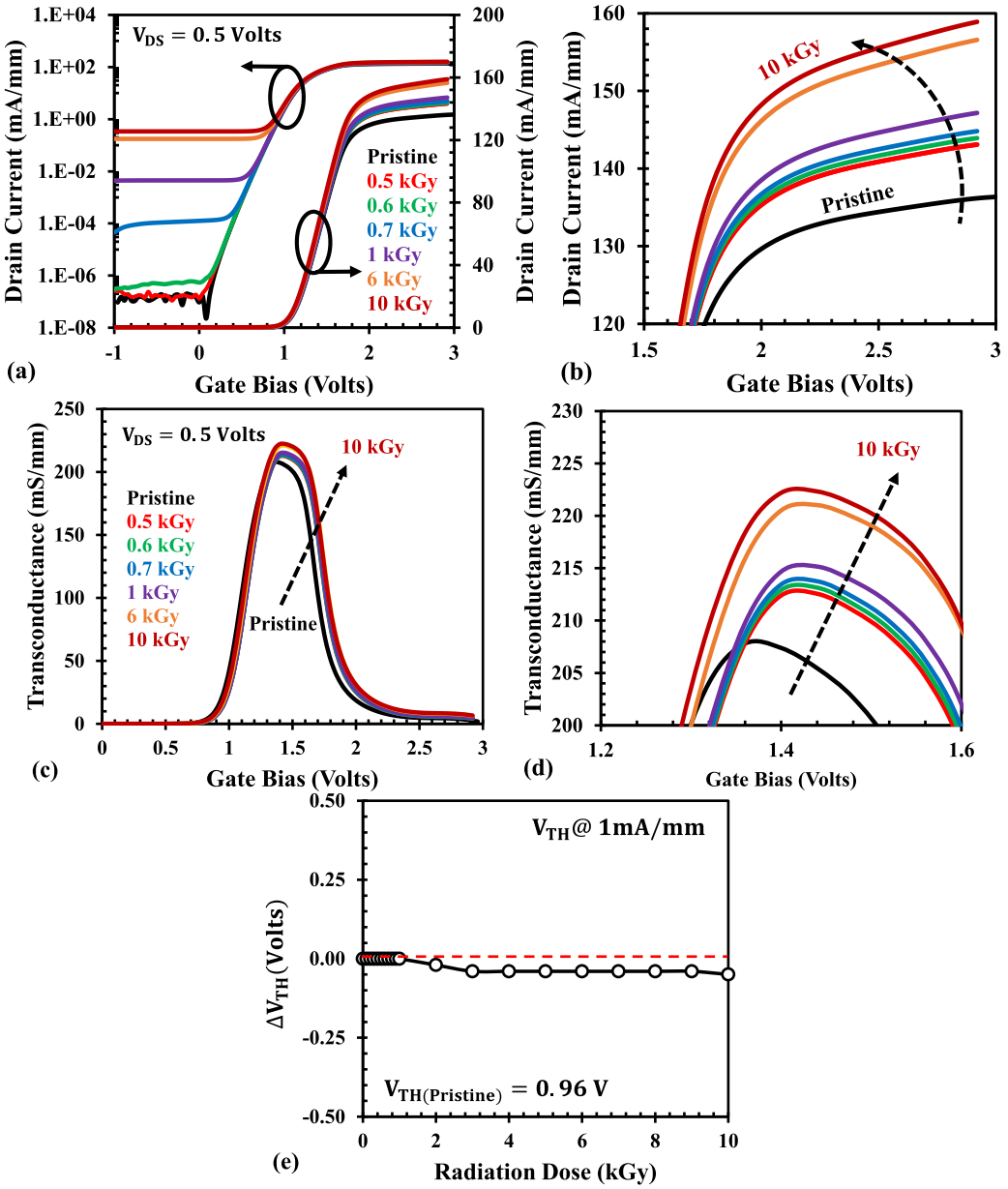

FIGURE 5. Impact of γ – ray irradiation on Transfer characteristics in (a) Normal, and (b) Enlarged View, and Transconductance profile in (c) Normal, (d) Enlarged View, and (e) Threshold voltage shift (ΔV_{TH}) as a function of TID level. All the terminals of the DUT were grounded during the exposure to mimic the experimental setup as per [26]–[28].

piezoelectric coefficients and structural reordering [32], [47] or through the improvement in the surface roughness [31]. Annealing of active traps post irradiation [48] and subsequent generation of interstitial/point defects in the form of nitrogen vacancies acting as donors [30] can also improve the carrier densities. Apart from these, reduction in the channel resistance [30]–[32] or decrease in activation energy coupled with an increase in the minority carrier diffusion lengths [49], [50] has also been observed to improve the drain current of the device.

The graded AlGaN layers housing the 3DEG channel can exhibit higher carrier mobilities due to the absence of impurity scattering [9]. The enhancement in drain current observed from Fig. 5 (a-b) points towards the possibility of enhancement in carrier mobilities to be the dominant reason for the observed effects, which gets translated towards the increase in peak transconductance as depicted in Fig. 5 (c-d). Further, since a major area of the DUT in the form of access regions is being exposed to direct interaction with the γ – Rays, the charge buildup consequently disrupts the 2DHG at the GaN top layer. This eventually aids the 3DEG carrier concentration in the positively graded AlGaN layer. The control for the depletion of 2DHG, however, remains with the Gate electrode. As the gate bias is raised above the threshold voltage, the conduction band is pulled below the fermi level, which pulls the electrons, consequently developing an electron accumulation layer (EAL) at the sidewalls of the trench gate [14], [19], [20]. This essentially depletes the 2DHG at the interface of GaN(top)/AlGaN near the gate electrode and opens up a conducting path for the carriers from Source to Drain electrode. It is for this reason, the threshold voltage shift associated with γ – irradiation is negligible for the DUT even at a higher dose, as depicted in Fig. 5(e).

Since a major portion of the access region of the device is exposed, there is also a high possibility of active traps being annealed due to the interaction with energetic photons. The heat generation, in essence, can be estimated by the formulation given by William *et al.* [51], as per Equation 1.

$$H_\gamma = c.E_\gamma.\mu_\gamma.\phi_\gamma \tag{1}$$

where, c is the conversion factor equal to 1.6×10^{-13}WsMeV^{-1}, E_γ is the energy of the γ – Rays in MeV, μ_γ is the linear absorption coefficient corresponding to γ – Rays with energy E_γ given in cm^{-1}, and ϕ_γ is the photon flux density corresponding to the γ – Rays with energy E_γ given in cm^{-2}s^{-1}. Further, the thermal conductivity κ (in Wcm^{-1}°C^{-1}) relates the heat transfer $(\Delta Q/\Delta T)$ and temperature gradient $(\Delta T/\Delta x)$ as per Equation 2.

$$\frac{\Delta Q}{\Delta t.A} = -\kappa\frac{\Delta T}{\Delta x} \tag{2}$$

Using Equations 1 and 2, with μ_γ and ϕ_γ as 0.33 cm^{-1} and 10^{15} cm^{-2}s^{-1} respectively [30], the average temperature change (ΔT) is estimated to be $\approx$ 184 °C at the positively graded AlGaN layer, which is in line with the earlier reports [30], [52]. This annealing effect has been captured in TCAD simulations using a thermal model associated with the insulator charging for the charge buildup, as demonstrated by Sehra *et al.* [24]. The annealing effects due to the energy transfer from the energetic γ – Ray photons leads to crystal reordering. This is responsible for the sudden jumps observed in ON – State and OFF – State currents for the initial dose (Fig. 5(a)), which starts saturating as the γ – Ray dose is increased. The electron – hole pairs generated post irradiation rearranges under the applied electric field. It aids the conducting path through the positive graded AlGaN towards the Source electrode via EAL at the sidewalls and GaN top layer.

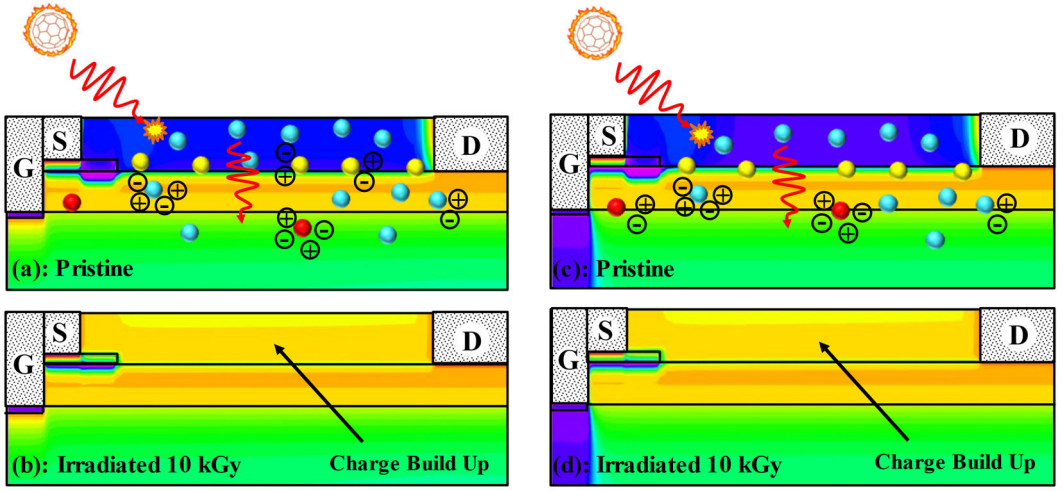

FIGURE 6. Electron concentration contour plots (Log Scale) for device in ON state (V_{GS} = 3 V and V_{DS} = 0.5 V) under (a) Pristine, and (b) 10 kGy irradiated; in OFF state (V_{GS} = −1 V and V_{DS} = 0.5 V) under (c) Pristine, and (b) 10 kGy irradiated. Positive (+) and Negative (-) symbols indicate the EHP generated after the interaction of Compton electrons with different energies (● ● ●) with the material.

This is depicted in Fig. 7(a) for brevity. The leakage paths in OFF – state post irradiation is depicted in Fig. 7(b).

It has also been reported that the degradation of the Schottky gate contact results in an increase of gate leakage current [23], [28]–[32], [49], [53]. As opposed to the common trend, some experimental studies have reported conflicting results demonstrating degradation of the drain current [49] or marginal improvement in the gate leakage current post irradiation [47]. Consequently, the interaction of γ – Rays on the device characteristics and the radiation induced traps so evolved are dependent upon a number of factors, including the quality of grown epi – layers. Further, the increase in OFF – state current recorded with γ – irradiation (as shown in Fig. 5(a)) is again linked with the insulator charging that disrupts the 2DHG at GaN top layer as observed in Fig. 6(d). This has a direct consequence in establishing a charge transfer in accordance with the trap assisted tunnelling (TAT). The TAT is dictated by the evolution of radiation induced traps that favor hole trapping due to a reduction in the barrier height [28]–[32], [49], [53], [54]. It effectively reduces the channel depletion as observed under the Source electrode at GaN top and graded AlGaN layers. In essence, it provides a leakage path from the GaN top layer to the positive graded AlGaN layers. Apart from these, the charge buildup in the insulator provides a leakage path, assisted by surface states on the GaN top and positive graded AlGaN layers, which is directly responsible for the increase in OFF – state leakage current (as shown in Fig. 5(a)).

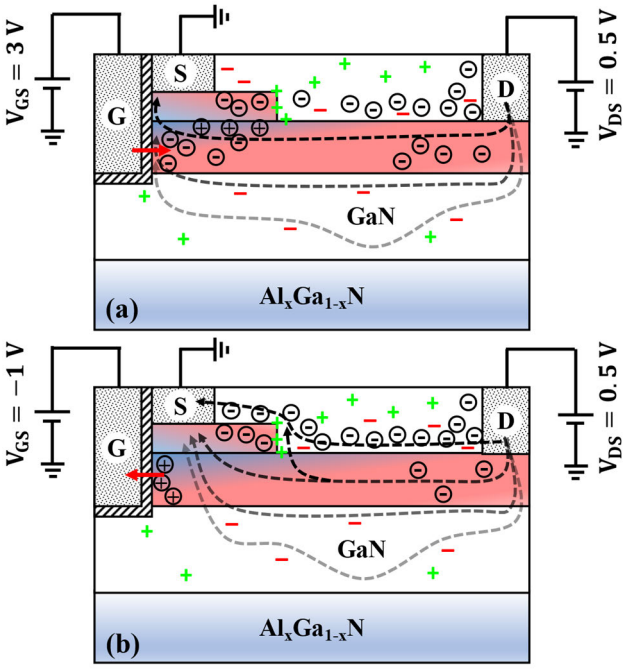

FIGURE 7. Schematic diagram depicting the γ – Ray induced electron – hole pairs driven by the electric fields setup due to the applied bias for (a) ON – State Condition (V_{GS} = 3 V and V_{DS} = 0.5 V), and OFF – State Condition (V_{GS} = −1 V and V_{DS} = 0.5 V). [→/(Dashed→): Electric Field/ Current Direction, +/−: Trapped Holes/ Electrons, (+)/(-): Excited Holes/ Electrons, / : Depicts 3DEG and 3DHG].

C. SENSITIVITY ASSESSMENT

To analyze the sensitivity of the DUT towards the ionizing radiation, DC characteristics of the device has been extracted as a function of γ – Ray dose at each stage. The ON – state and OFF – state currents recorded at V_{GS} = 3 V and V_{GS} = −1 V, respectively, are shown in Fig. 8(a), while the peak transconductance is shown in Fig. 8(b). The choice for V_{GS} = −1 V for OFF – state is taken in accordance with the saturation observed in OFF – state current (as observed from log scale in Fig. 5(a)). Further, V_{DS} has been set at 0.5 V in lines with the TCAD calibrations (Fig. 4). In conjunction with the explanation provided in the previous section, the enhancement in ON – state current initially exhibits a fairly linear operation at a low dose, and eventually proceeds towards saturation with a higher dose. This is due to the saturation in the enhancement of the carrier mobilities and traps being annealed out due to the interaction with the energetic photons.

The saturation in ON – state currents with increasing γ – Ray dose can also be linked with the fact that there is an incessant increase in the defect density with the γ – Ray dose. The increase in carrier mobilities is dominated primarily by the relaxation in film strain, increase in diffusion lengths, or active trap annealing for the lower doses. For the higher dose, however, the impurity scattering becomes dominant due to higher defect densities. This leads to the degradation of the carrier mobilities and hence the diffusion lengths. At this point, the contribution from the other factors discussed in the previous section, negate the effect of mobility degradation, as a result of which a saturation in the ON – state current is observed. A similar effect has been experimentally observed by Lee *et al.* [50], where a linear increase in diffusion lengths has been recorded for the low doses up to 200 Gy. This correlates well with the observed trend in I_{ON} for the doses up to 1 kGy as shown in Fig. 8(a), which is eventually translated into $g_{M(max)}$ as shown in Fig. 8(b). A close observation into Fig. 8(a) demonstrates a linear increase in OFF – state current with γ – Ray doses above 1 kGy. Contour plots of electron concentration depicted in Fig. 6(d) at 10 kGy demonstrate the insulator's charge buildup that aids the reverse leakage

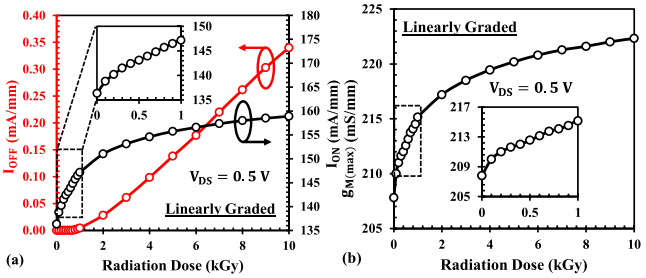

FIGURE 8. Influence of γ – Ray irradiation on the (a) ON – State / OFF – state currents and on the (b) Peak Transconductance for Linearly Graded AlGaN layers.

current through the surface states available on the GaN top and graded AlGaN layers.

To illustrate this, the evolution of leakage paths with different γ – dose through the device is shown in Fig. 9 (a)-(d) using conduction current density contours under pristine state and for different dose. It is evident from the contour plots of Fig. 9 (a)-(d), that, as the irradiation dose is increased from 2kGy to 8kGy, there is a prominent leakage path from the 3DEG housed by positive graded AlGaN layer towards the Source electrode as compared to the pristine state (Fig. 9(a)). The leakage path is a consequence of the TAT and hopping mechanisms due to the available surface states along the sidewalls of the GaN top layer. As the dose increases, the carrier injection and carrier hopping become more significant, increasing the leakage area near the sidewalls of the GaN top layer, as shown in Fig. 9(d). This is in conjunction with the EHP driven by the electric fields, shown in Fig. 7(b). The leakage area is expected to get broader with the γ – Ray dose until the region reaches the Drain electrode. At this point, there will be a direct injection of the carriers between Source and Drain electrodes via the passivation layer, consequently resulting in a premature breakdown of the device.

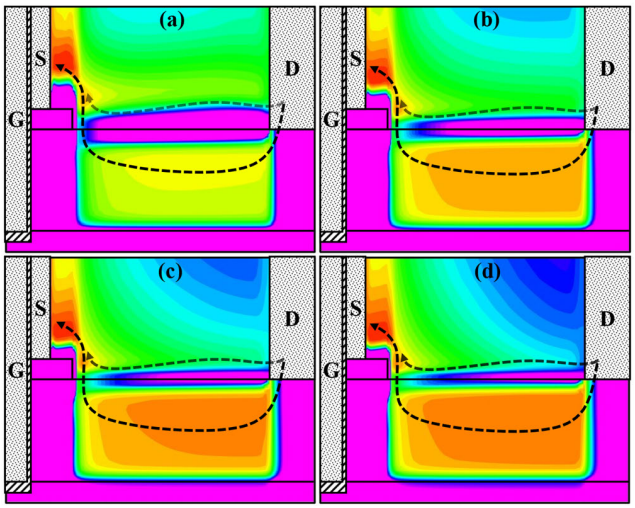

FIGURE 9. Evolution of conduction current density (A/cm^2) in log scale for γ – Ray dose at (a) 2 kGy, (b) 4 kGy, (c) 6 kGy, and (d) 8 kGy. Device is biased in OFF – State condition ($V_{GS} = -1$ V and $V_{DS} = 0.5$ V).

To sum up, the increase in I_{ON} and I_{OFF} recorded as a function of γ – Ray dose, for the said DUT can be exploited for dosimeter applications. The device exhibits linear characteristics with regards to the increase in I_{ON} for γ – Ray doses up to 1 kGy. This points towards a higher sensitivity of the device towards the early detection of low dose γ – Rays. In addition to this, the device as observed also demonstrates a linear trend in I_{OFF} with cumulative dose γ – Ray effects, pointing towards the compatibility of the DUT for the detection of high dose γ – Rays as well. Finally, a high stability of the resulting dosimeter can be established primarily due to the negligible shifts in the device threshold voltage even at a higher dose. As a consequence, the operating conditions of the dosimeter remains intact. In addition, experimental reports [54], [55] suggest the recovery of such irradiated samples post high temperature annealing process, which adds up to the stability of the DUT for dosimetry applications.

D. SENSITIVITY OPTIMIZATION USING GRADED PROFILES

The graded channel HEMTs have been observed to offer improved linearity and lower intermodulation distortion by tailoring their transconductance characteristics to achieve a broader profile [10]–[12]. This is in contrast to the fact that the grading may in fact be tailored by controlling the flow of trimethylgallium (TMG - $Ga(CH_3)_3$) and trimethylaluminum (TMAl - $Al_2(CH_3)_6$) precursors during growth in an MOCVD Chamber. To this extent, there have been several reports that explore other grading profiles for various applications which include the square root [56] and parabolic grading [57] for improved linearity for LNA applications. Parabolic and S – graded (ERFC profile) buffer layers have also been used for reducing threading dislocations [58], [59] in various optoelectronic applications [60]. In this regard, the performance of such graded profiles is further explored for dosimetry based on the original structure. Venkatesan *et al.* [56] have demonstrated an improvement in the linearity performance of the device comes with a trade off in the drain current metrics. This trade off can be linked with the fact that the resulting electron profile in the channel ($\sigma_{Channel}$) is dependent upon the divergence of polarization field (P_{Pol}) along the growth direction, as dictated by Equation 3 [8], [9].

$$\sigma_{Channel} = \nabla \cdot P_{Pol} \tag{3}$$

In this regard, a linear graded profile will render a uniform profile, and a parabolic grading will yield a linear variation of electron concentration across the entire AlGaN layer.

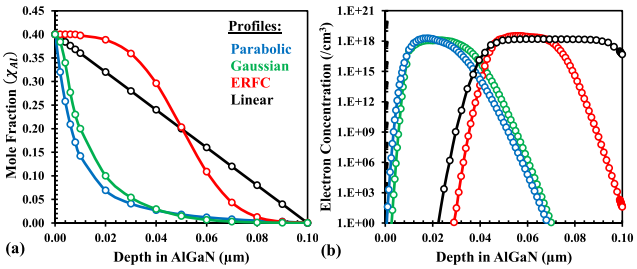

FIGURE 10. Comparison of (a) Different Graded Profiles in positively graded AlGaN layer, and (b) Resulting Electron Concentration plots as a function of layer depth.

Additionally, gaussian grading would result in electron concentration that follows $2x.e^{-x^2}$, assuming the peak is centered at zero with a standard deviation of $1/\sqrt{2}$ and S – shaped (i.e., erfc) would follow a $2.e^{-x^2}/\sqrt{\pi}$ variation. Since the polarization field depends on the contributions from both the spontaneous and piezoelectric coefficients, the resulting profiles will be approximate [8], [9]. A depiction of

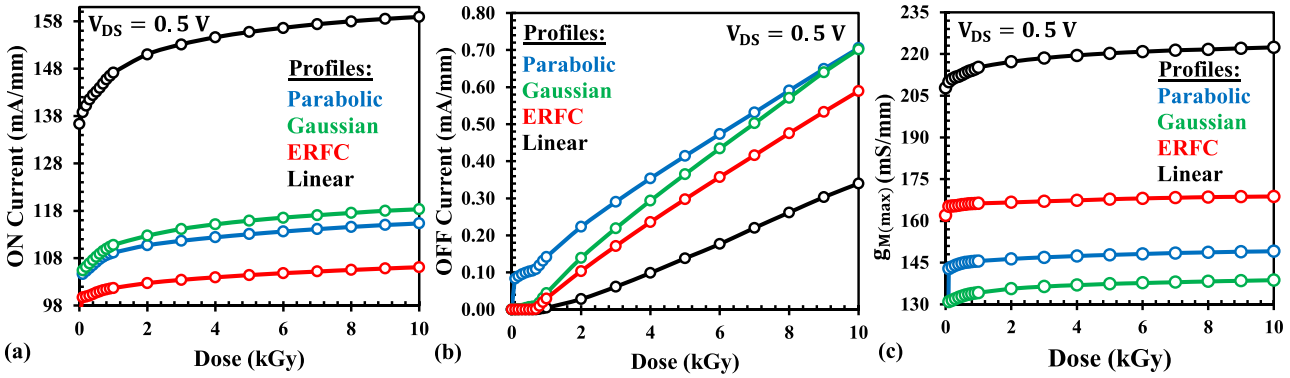

FIGURE 11. Influence of γ – Ray irradiation on the (a) ON – State Current, (b) OFF – state Current, and (c) Peak Transconductance for different grading profiles of AlGaN layer.

the different grading profiles and the resulting electron concentrations is shown in Fig. 10(a) and Fig. 10(b), respectively, and agrees with Equation 3. These profiles are investigated for dosimetry under cumulative dose γ – Ray irradiation effects.

The effect of cumulative dose γ – Ray irradiation on the evolution of ON – and OFF – state drain current along with the impact on device transconductance for all the graded profiles (i.e. Parabolic, Gaussian, ERFC and Linear) is depicted in Fig. 11(a-c), respectively. A significant impact on the trends of ON – and OFF – state currents is observed with different graded profiles as shown in Fig. 11 (a-b). The trends of peak transconductance follow closely to that of ON – state current and gets saturated early from low dose γ - rays (Fig. 11(c)). As expected, all the profiles exhibit a similar trend in the I_{ON} and I_{OFF} with γ – Ray dose, and suggests the possibility of detecting low and high dose γ – Rays. The conduction paths for the parabolic profile for both ON – State and OFF – State conditions under linear variation is depicted in Fig. 12(a-b) and Fig. 12(c-d), respectively at a different dose.

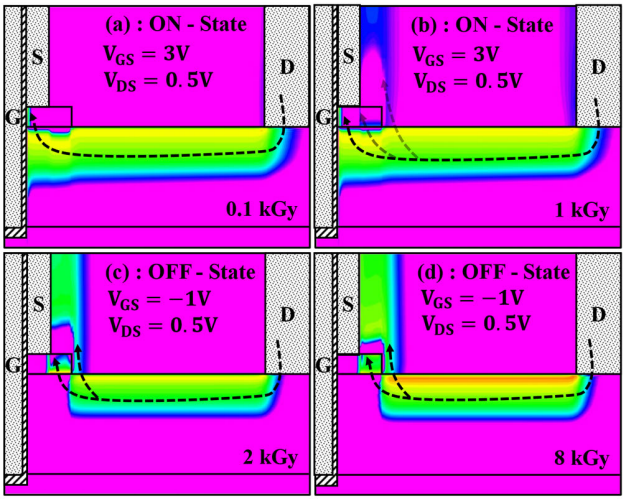

FIGURE 12. Evolution of conduction current density (A/cm^2) in log scale for γ – Ray dose at (a) 0.1 kGy, (b) 1 kGy in ON – State Condition (V_{GS} = 3 V and V_{DS} = 0.5 V), and (c) 2 kGy, (d) 8 kGy in OFF – State Condition (V_{GS} = −1 V and V_{DS}= 0.5 V). AlGaN layers are parabolic graded.

As observed from Fig. 12(a-b) for low dose γ – Rays up to 1 kGy, the dominant path for the conduction current is through the formation of EAL at the sidewalls of the trench gate in the parabolic graded AlGaN and GaN top layers. As the dose increases, two conduction paths are observed (shown in Fig. 12(b)). One is due to a spillover and carrier injection from parabolic graded AlGaN into GaN top layer, which depletes the 2DHG. The other path is carved out in the passivation layer through the charge buildup, courtesy of the Compton electrons. However, the increase in defect densities limits the carrier diffusion lengths and the carrier mobilities, as discussed in the previous section. The increase in I_{ON} thus gets saturated as the investigation proceeds towards a higher dose. However, in the OFF – state condition, a new dominant leakage path emerges out through the GaN top layer compared with the linear counterpart. This can be understood from the electron concentration plots compiled in Fig. 10(a). The peak in carrier concentration for parabolic graded profile occurs in the vicinity of the GaN top layer, which houses the 2DHG to realize enhancement mode operation. The carrier injection, in this case, aided by the TAT through the trapping states evolved in GaN top layer is dominant due to a spillover of the charge carriers into the GaN top layer. This eventually depletes the 2DHG at the region not covered by the Source electrode. As a consequence of this, a new conduction path in the OFF – state condition emerges (shown in Fig. 12 (c-d)) that aids the drain current (I_{OFF}) in the absence of EAL and presence of 2DHG at the trench gate and GaN top layers, respectively. A linear variation in I_{OFF} is thus observed for the higher dose γ – Rays (shown in 11 (b)).

Current density contour plots recorded under ON – State and OFF – State conditions for low and high dose γ – Rays to investigate the conduction paths for gaussian graded AlGaN layer is shown in Fig 13 (a-d). Fig. 13(a-b) depicts the conduction paths under ON – State and low dose γ – Rays, and in Fig. 13(c-d) under OFF – State and high dose γ – Rays. The conduction paths under ON – State, as observed from

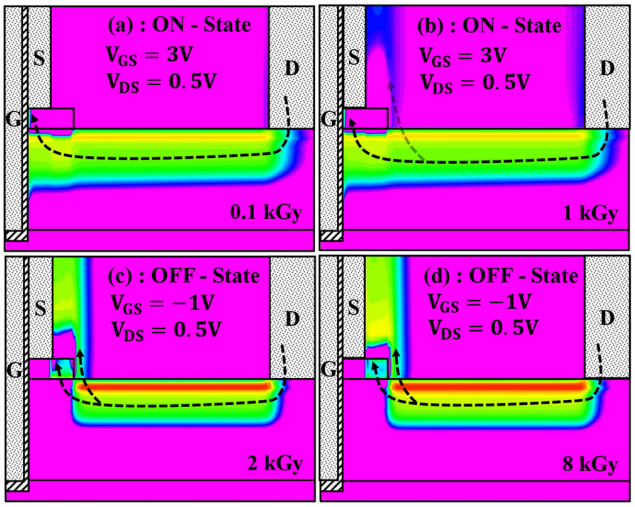

FIGURE 13. Evolution of conduction current density (A/cm^2) in log scale for γ – Ray dose at (a) 0.1 kGy, (b) 1 kGy in ON – State Condition (V_{GS} = 3 V and V_{DS} = 0.5 V), and (c) 2 kGy, (d) 8 kGy in OFF – State Condition (V_{GS} = −1 V and V_{DS} = 0.5 V). AlGaN layers are gaussian graded.

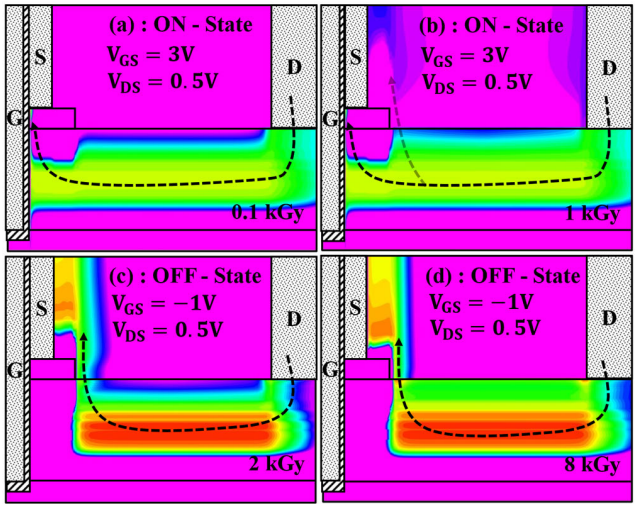

FIGURE 14. Evolution of conduction current density (A/cm2) in log scale for γ – Ray dose at (a) 0.1 kGy, (b) 1 kGy in ON – State Condition (V_{GS} = 3 V and V_{DS} = 0.5 V), and (c) 2 kGy, (d) 8 kGy in OFF – State Condition (V_{GS} = −1 V and V_{DS} = 0.5 V). AlGaN layers are ERFC graded.

Fig. 13(a-b) are similar to the ones recorded for parabolic graded in Fig. 12(a-b), except that the spillover effect is not observed (as seen in Fig. 13(b)). However, under OFF – state conditions (in Fig. 13(c-d)), the EHP generation aided by the Compton electrons produced from high dose γ – Rays result in an excitation of electrons. Under the applied bias, this aids the charge spillover into the GaN top layer from the graded AlGaN layers. This charge sharing is again facilitated by the vicinity of peak electron concentrations near the GaN(top)/AlGaN interface (as depicted in Fig. 10(b)).

The contour plots of conduction current density depicting the current paths for the resulting DUT for ERFC graded AlGaN is depicted in Fig. 14 (a-d). The current paths for the ON – State biased device at a low dose as shown in Fig. 14(a-b) correspond to that of a linear graded AlGaN layer, except that the spread of 3DEG charge is limited compared to its linear counterpart. This correlates well with the electron concentration plots as a function of AlGaN depth depicted in Fig. 10(b). The dominant conduction path for ERFC graded AlGaN under low dose γ - Rays remains similar to the other profiles investigated. However, the conduction current through the passivation layer is negligible, identical to that of its linear counterpart. This is primarily due to the shift in peak electron concentration away from the GaN(top)/AlGaN interface (as depicted in Fig. 10(b)). Under OFF – State conditions, since, the peak in electron concentration is centered away from the interface, the spillover of excited electrons to the GaN top layer is not observed. As a result, the current leakage paths are similar to the linear profile shown in Fig. 9. As observed from Fig. 14(c-d), the dominant leakage paths in OFF – State (for ERFC graded AlGaN) have a dominant path due to the hopping from the available surface traps and the TAT through the trapping states that evolved under high dose γ – Rays.

E. COMPARISON OF SENSITIVITY TOWARDS γ – RAY DOSE

This section gives a numerical insight into the dosimeter sensitivity based on the different grading profiles investigated in the previous section. The analysis is divided into two parts, i.e. considering the best-case scenarios for detecting low dose and high dose γ – Rays. The sensitivity of the device to the γ – Ray dose can be modeled directly by recording the change in drain current with the cumulative γ – Ray dose at each stage. Mathematically, this can be represented by Equation 4.

$$S_{\gamma-Ray} = \frac{I_{IrradiatedS2} - I_{IrradiatedS1}}{D_{Stage2} - D_{Stage1}} \tag{4}$$

where, $S_{\gamma-Ray}$ is the sensitivity of the device (in mA/mm/kGy) to the incident γ – Rays, $I_{IrradiatedS2}$ and $I_{IrradiatedS1}$ are the resulting currents (in mA/mm) post irradiation at doses (in kGy) D_{Stage2} and D_{Stage1} respectively.

To evaluate sensitivity with respect to the pristine conditions, D_{Stage1} is set to 0 kGy to indicate pristine condition. On the basis of these, curve fitting techniques are used to evaluate the overall sensitivity of the device for the low and high dose γ – Rays. A comparison of all the profiles investigated for the early detection of low dose γ – Rays using I_{ON} is depicted in Fig. 15(a), and for the detection of high dose γ – Rays using I_{OFF} is shown in Fig. 15(b). The sensitivity metric dictated by Equation 4 and extracted from Fig. 15 (a) and (b) is compared for all the different profiles and summarized in Table 3.

A superficial look into Table 3 shows that the linear profile is best suited for detecting low dose γ – Rays. However, on investigating the Coefficient of Determination (R^2 Value) and Pearson's Correlation Coefficient (Pearson's R), it is revealed that the gaussian graded profile follows a more linear

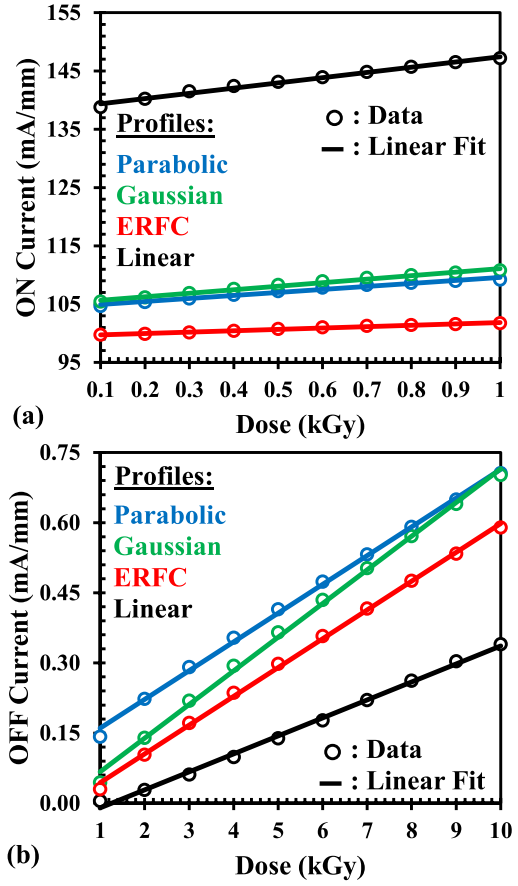

FIGURE 15. Drain current evolution of different grading profiles for the detection of (a) low dose γ – Rays under ON – State Conditions, and (b) high dose γ – Rays under OFF – State.

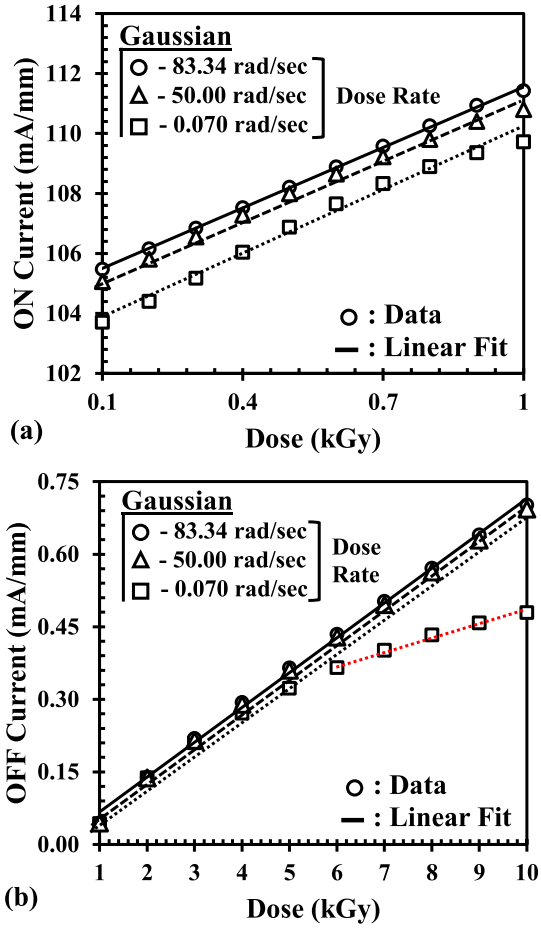

FIGURE 16. Drain current evolution of gaussian grading profile under different dose rates for the detection of (a) low dose γ – Rays under ON – State Conditions, and (b) high dose γ – Rays under OFF – State.

TABLE 3. Comparison of sensitivity metrics extracted from different grading profiles at V_{DS} = 0.5 V.

Condition	Profiles	Sensitivity	R^2 Value	Pearson's R
Low Dose γ – Rays [0.1 – 1 kGy]	Linear	8.99 mA/mm/kGy	0.989	0.995
	Parabolic	5.52 mA/mm/kGy	0.987	0.993
	Gaussian	**6.32 mA/mm/kGy**	**0.993**	**0.996**
	ERFC	2.46 mA/mm/kGy	0.992	0.995
High Dose γ – Rays [1 – 10 kGy]	Linear	0.0385 mA/mm/kGy	0.979	0.989
	Parabolic	0.0615 mA/mm/kGy	0.989	0.997
	Gaussian	**0.072 mA/mm/kGy**	**0.997**	**0.998**
	ERFC	0.0616 mA/mm/kGy	0.996	0.997

approach towards the dosimetry. This is observed for the case of higher dose γ – Rays as well. For standalone dosimeters, the linear graded and gaussian graded profiles are best suited for detecting low and high dose γ – Rays, respectively. However, for generic dosimetry, for the detection of both low and high dose γ – Rays, gaussian graded profiles gives the best performance in terms of both the sensitivity to ionizing radiation and following a linear approach.

F. DOSE RATE EFFECTS ON SENSITIVITY OF γ – RAY DOSIMETER

Literature survey suggests the presence of high defect densities in oxide layers in bipolar devices and ICs to be responsible for the enhanced sensitivity observed when irradiated at lower electric fields [61]–[65]. This phenomenon is commonly referred to as Enhanced Low Dose Rate Sensitivity (ELDRS) [61]–[65]. Accordingly, it is imperative to investigate the device under such environments and comment about its sensitivity capabilities. In this regard, the 3DEG HEMT as a dosimeter is further evaluated under different dose rate conditions as the radiation environment where the dosimeter is employed will be different. Accordingly, the best - case scenario identified in Section 3.5 is investigated under a ^{60}Co source with a dose rate of 0.07 rad/sec [28] and 50 rad/sec [29]. The sensitivity profiles of a gaussian graded 3DEG HEMT for the detection of low dose γ – Rays using I_{ON} is depicted in Fig. 16(a), and for the detection of high dose γ – Rays using I_{OFF} is shown in Fig. 16(b). The sensitivity metrics for the linear region are compiled in Table 4. A parallel shift in the trend of ON and OFF state currents with low and high dose γ – Rays are observed in Fig. 16(a) and Fig. 16(b), respectively, considering dose rates of 50 rad/sec and 0.07 rad/sec. This suggests that the dosimeter sensitivity is not significantly affected even with low and mid – range dose rates as compiled in Table 4.

TABLE 4. Comparison of sensitivity metrics evaluated at different dose rates for the gaussian graded profile at $V_{DS} = 0.5$ Volts.

Condition	Dose Rate	Sensitivity	R^2 Value	Pearson's R
Low Dose	83.34 rad/sec	6.32 mA/mm/kGy	0.993	0.996
γ – Rays	50.00 rad/sec	6.45 mA/mm/kGy	0.994	0.997
[0.1 – 1 kGy]	0.070 rad/sec	6.97 mA/mm/kGy	0.988	0.992
High Dose	83.34 rad/sec	0.072 mA/mm/kGy	0.997	0.998
γ – Rays	50.00 rad/sec	0.071 mA/mm/kGy	0.997	0.998
[1 – 10 kGy]	0.070 rad/sec	0.069 mA/mm/kGy	0.985	0.992

The slight change in sensitivity recorded for 50 rad/sec and 0.07 rad/sec is due to the spread of the annealing effect from the energetic photons which is significantly reduced due to the photon flux density at low dose rates [51], [66]. This will also lead to the early saturation observed in the OFF – state current at a low dose rate of 0.07 rad/sec and considering high dose γ – Rays as shown in Fig. 16 (b).

At a lower dose rate (0.07 rad/sec), a significant amount of time is required for irradiating the devices at a high dose of γ – Rays (for 6 kGy $\sim$ 100 Days at 0.07 rad/sec), during which the trapped carriers get emitted at various instances depending upon their time constants. As a consequence of this, early saturation is observed in OFF – state current from 6 kGy onwards, as depicted in Fig. 16(b). In this regard, the sensitivity metric for the detection of high dose γ – Rays at a lower dose rate (i.e., 0.07 rad/sec) corresponds to a range up to 6 kGy. Further, the R^2 Value and Pearson's R coefficient compiled in Table 4 remains close to unity, thereby validating the linearity of the 3DEG HEMT for dosimeter applications. Moreover, since the sensitivity metrics are not significantly affected at lower dose rates, it can be suggested that the ELDRS effect is not observed in the device under test. This is also in agreement with the experimental results reported by Jiang *et al.* [28] which evinces that such an effect is due to the high electric field exhibited by GaN devices compared to the bipolar base oxides [64], [65]. Since the interaction between the radiation induced traps with the electron/hole/proton transport (which dictates ELDRS effect) is fundamentally different in crystalline wide – bandgap GaN compared to amorphous SiO_2 [28], [63], and due to the strong bonding nature of III – V binary and ternary nitrides [21]–[24], the ELDRS effect is not prominent in such devices.

IV. CONCLUSION

A HEMT device architecture exhibiting positive and negative graded AlGaN layers supporting 3DEG for conduction and 3DHG for back barrier is investigated for dosimeter applications. The key takeaway points from the detailed analysis are as follows. The linear variation recorded in I_{ON} with γ – Ray irradiation validates the device architecture for the early detection of low dose γ – Rays. The device architecture, as investigated, exhibits a linear variation in I_{OFF} for the detection of high dose γ – Rays as well. The negligible shift observed in the device threshold voltage even for higher dose γ – Rays validates the stability of the operating conditions for the proposed dosimetry. A detailed physical insight towards the irradiation effects on the device has been presented with the validation from the experimental sources to establish the device for stable dosimeter applications. Finally, the sensitivity of the device has been optimized by investigating different grading profiles for the best-case scenarios. On that account, the gaussian graded profile has been identified as the best-case scenario regarding the sensitivity and exhibiting a linear operation.

ACKNOWLEDGMENT

The authors would also like to thank B.Sc. (Hons.) Electronics Students at the Deen Dayal Upadhyaya College, University of Delhi: Raghvendra Pratap Singh (19HEL2039, Fifth Semester, Batch: 2019–2022) and Sharat Singh (20HEL2142, Third Semester, Batch: 2020–2023) for confirming the results through Keysight ADS.

REFERENCES

[1] V. K. Pandey and C. M. Tan, "Application of gallium nitride technology in particle therapy imaging," *IEEE Trans. Nucl. Sci.*, vol. 68, no. 6, pp. 1319–1324, Jun. 2021, doi: 10.1109/TNS.2021.3072654.
[2] L. H. Hsu, Y. Y. Lai, T. P. Tu, C. Langpoklakpam, T. Y. Chang, H. W. Yu, W. Lee, J. Tzou, Y. Cheng, C. Lin, H. Kuo, and E. Chang, "Development of GaN HEMTs fabricated on silicon, silicon-on-insulator, and engineered substrates and the heterogeneous integration," *Micromachines*, vol. 12, no. 10, pp. 1–32, 2021, doi: 10.3390/mi12101159.
[3] D. Y. C. Lie, J. Tsay, T. Hall, T. Nukala, and J. Lopez, "High-efficiency silicon RF power amplifier design—Current status and future outlook," in *Proc. IEEE Int. Symp. Radio-Freq. Integr. Technol. (RFIT)*, May 2016, pp. 1–4, doi: 10.1109/RFIT.2016.7578181.
[4] T. McDonald and S. W. Butler, "Progress and current topics of JEDEC JC-70.1 power GaN device quality and reliability standards activity: Or: What is the avalanche capability of your GaN transistor?" in *Proc. Int. Rel. Phys. Symp.*, 2021, pp. 1–6, doi: 10.1109/IRPS46558.2021.9405225.
[5] R. Mitova, R. Ghosh, U. Mhaskar, D. Klikic, M. X. Wang, and A. Dentella, "Investigations of 600-V GaN HEMT and GaN diode for power converter applications," *IEEE Trans. Power Electron.*, vol. 29, no. 5, pp. 2441–2451, Dec. 2013, doi: 10.1109/TPEL.2013.2286639.
[6] K. J. Chen, O. Häberlen, A. Lidow, C. L. Tsai, T. Ueda, Y. Uemoto, and Y. Wu, "GaN-on-Si power technology: Devices and applications," *IEEE Trans. Electron Devices*, vol. 64, no. 3, pp. 779–795, Mar. 2017, doi: 10.1109/TED.2017.2657579.
[7] J. P. Ibbetson, P. T. Fini, K. D. Ness, S. P. DenBaars, J. S. Speck, and U. K. Mishra, "Polarization effects, surface states, and the source of electrons in AlGaN/GaN heterostructure field effect transistors," *Appl. Phys. Lett.*, vol. 77, no. 2, pp. 250–252, 2000, doi: 10.1063/1.126940.
[8] D. Jena, S. Heikman, D. Green, D. Buttari, R. Coffie, H. Xing, S. Keller, S. DenBaars, J. S. Speck, U. K. Mishra, and I. Smorchkova, "Realization of wide electron slabs by polarization bulk doping in graded III–V nitride semiconductor alloys," *Appl. Phys. Lett.*, vol. 81, no. 23, pp. 4395–4397, Dec. 2002, doi: 10.1063/1.1526161.
[9] S. Rajan, H. Xing, S. DenBaars, U. K. Mishra, and D. Jena, "AlGaN/GaN polarization-doped field-effect transistor for microwave power applications," *Appl. Phys. Lett.*, vol. 84, no. 9, pp. 1591–1593, Jan. 2004, doi: 10.1063/1.1652254.
[10] P. S. Park, D. N. Nath, S. Krishnamoorthy, and S. Rajan, "Electron gas dimensionality engineering in AlGaN/GaN high electron mobility transistors using polarization," *Appl. Phys. Lett.*, vol. 100, no. 6, 2012, Art. no. 063507, doi: 10.1063/1.3685483.
[11] S. Bajaj, Z. Yang, F. Akyol, P. S. Park, Y. Zhang, S. H. Sohel, S. Krishnamoorthy, D. J. Meyer, and S. Rajan, "Small-signal characteristics of graded AlGaN channel PolFETs," in *Proc. Annu. Device Res. Conf. (DRC)*, 2017, pp. 1–2, doi: 10.1109/DRC.2017.7999409.
[12] S. Bajaj, Z. Yang, F. Akyol, P. S. Park, Y. Zhang, A. L. Price, S. Krishnamoorthy, D. J. Meyer, and S. Rajan, "Graded AlGaN channel transistors for improved current and power gain linearity," *IEEE Trans. Electron Devices*, vol. 64, no. 8, pp. 3114–3119, Aug. 2017, doi: 10.1109/TED.2017.2713784.

[13] B. Hou, L. Yang, M. Mi, M. Zhang, C. Yi, M. Wu, Q. Zhu, Y. Lu, J. Zhu, and X. Zhou, "High linearity and high power performance with barrier layer of sandwich structure and $Al_{0.05}GaN$ back barrier for X-band application," *J. Phys. D, Appl. Phys.*, vol. 53, no. 14, 2020, Art. no. 145102, doi: 10.1088/1361-6463/ab678f.

[14] X. Luo, F. Peng, C. Yang, J. Wei, S. Deng, D. Ouyang, and B. Zhang, "Polarization-doped enhancement mode HEMT," U.S. Patent 10 304 931 B2, May 28,2019. Accessed: Jul. 20, 2021. [Online]. Available: https://patents.google.com/patent/US10304931B2/

[15] M. Ge, Y. Li, Y. Zhu, D. Chen, Z. Wang, and S. Tan, "Effects of gate work function on E-mode AlGaN/GaN HEMTs with stack gate β-Ga_2O_3/p-GaN structure," *J. Phys. D, Appl. Phys.*, vol. 54, no. 35, 2021, Art. no. 355103, doi: 10.1088/1361-6463/ac0a0b.

[16] M. Ge, Y. Li, Y. Zhu, D. Chen, Z. Wang, and S. Tan, "An improved design for e-mode AlGaN/GaN HEMT with gate stack β-Ga_2O_3/p-GaN structure," *J. Appl. Phys.*, vol. 130, no. 3, 2021, Art. no. 035703, doi: 10.1063/5.0051274.

[17] F. Wang, W. Chen, X. Li, R. Sun, X. Xu, Y. Xin, Z. Wang, Y. Shi, Y. Xia, and C. Liu, "Charge storage impact on input capacitance in p-GaN gate AlGaN/GaN power high-electron-mobility transistors," in *J. Phys. D, Appl. Phys.*, vol. 53, no. 30, 2020, Art. no. 305106, doi: 10.1088/1361-6463/ab86e7.

[18] R. Grady and C. Bayram, "Simulation of zincblende AlGaN/GaN high electron mobility transistors for normally-off operation," *J. Phys. D, Appl. Phys.*, vol. 50, no. 26, 2017, Art. no. 265104, doi: 10.1088/1361-6463/aa74fc.

[19] F. Peng, C. Yang, S. Deng, D. Ouyang, B. Zhang, J. Wei, and X. Luo, "Simulation of a high-performance enhancement-mode HFET with back-to-back graded AlGaN layers," *Sci. China Inf. Sci.*, vol. 62, no. 6, pp. 1–11, Jun. 2018, doi: 10.1007/s11432-018-9503-9.

[20] S. Deng, J. Wei, D. Ouyang, B. Zhang, C. Yang, and X. Luo, "High performance enhancement-mode HEMT with 3DEG to conduct current and 3DHG as back barrier," *Superlattices Microstructures*, vol. 130, pp. 437–445, Jun. 2019, doi: 10.1016/j.spmi.2019.04.024.

[21] A. Ionascut-Nedelcescu, C. Carlone, A. Houdayer, H. J. von Bardeleben, J.-L. Cantin, and S. Raymond, "Radiation hardness of gallium nitride," *IEEE Trans. Nucl. Sci.*, vol. 49, no. 6, pp. 2733–2738, Dec. 2002, doi: 10.1109/TNS.2002.805363.

[22] A. Y. Polyakov, S. J. Pearton, P. Frenzer, F. Ren, L. Liu, and J. Kim, "Radiation effects in GaN materials and devices," *J. Mater. Chem. C*, vol. 1, no. 5, pp. 877–887, Feb. 2013, doi: 10.1039/c2tc00039c.

[23] J. Pearton, F. Ren, E. Patrick, M. E. Law, and A. Y. Polyakov, "Ionizing radiation damage effects on GaN devices," *ECS J. Solid State Sci. Technol.*, vol. 5, no. 2, pp. 35–60, 2015, doi: 10.1149/2.0251602jss.

[24] K. Sehra, V. Kumari, M. Gupta, M. Mishra, D. S. Rawal, and M. Saxena, "TCAD investigation of total ionizing dose (TID) effects on gallium nitride HEMTs," in *Silvaco's Simul. Standard*, vol. 31, no. 1, pp. 1–6, 2021. Accessed: Jul. 20, 2021. [Online]. Available: https://silvaco.com/simulation-standard/tcad-investigation-of-total-ionizing-dose-tid-effects-on-gallium-nitride-hemts/

[25] C. Sharma, R. Laishram, D. S. Rawal, S. Vinayak, and R. Singh, "Cumulative dose 60Co gamma irradiation effects on AlGaN/GaN Schottky diodes and its area dependence," *Proc. AIP Conf. Proc.*, vol. 1942, no. 1, 2018, Art. no. 120015, doi: 10.1063/1.5029055.

[26] X. Sun, O. I. Saadat, J. Chen, E. X. Zhang, S. Cui, T. Palacios, D. M. Fleetwood, and T. P. Ma, "Total-ionizing-dose radiation effects in AlGaN/GaN HEMTs and MOS-HEMTs," *IEEE Trans. Nucl. Sci.*, vol. 60, no. 6, pp. 4074–4079, Dec. 2013, doi: 10.1109/TNS.2013.2278314.

[27] M. A. Bhuiyan, H. Zhou, S.-J. Chang, X. Lou, X. Gong, R. Jiang, H. Gong, E. X. Zhang, C.-H. Won, J.-W. Lim, J.-H. Lee, R. G. Gordon, R. A. Reed, D. M. Fleetwood, P. Ye, and T.-P. Ma, "Total-ionizing-dose responses of GaN-based HEMTs with different channel thicknesses and MOSHEMTs with epitaxial MgCaO as gate dielectric," *IEEE Trans. Nucl. Sci.*, vol. 65, no. 1, pp. 46–52, Jan. 2018, doi: 10.1109/TNS.2017.2774928.

[28] R. Jiang, E. Xia Zhang, M. W. McCurdy, P. Wang, H. Gong, D. Yan, R. D. Schrimpf, and D. M. Fleetwood, "Dose-rate dependence of the total-ionizing-dose response of GaN-based HEMTs," *IEEE Trans. Nucl. Sci.*, vol. 66, no. 1, pp. 170–176, Jan. 2019, doi: 10.1109/TNS.2018.2873059.

[29] S.-J. Chang and D. S. Kim, "Comprehensive research of total ionizing dose effects in GaN-based MIS-HEMTs using extremely thin gate dielectric layer," *Nanomaterials*, vol. 10, no. 11, pp. 1–11, 2020, doi: 10.3390/nano10112175.

[30] C. Sharma and N. Modolo, "Investigation of the degradations in power GaN-on-Si MIS-HEMTs subjected to cumulative γ-ray irradiation," *Microelectron. Rel.*, vols. 110–101, Jan. 2019, Art. no. 113349, doi: 10.1016/j.microrel.2019.06.041.

[31] C. Sharma, A. K. Visvkarma, R. Laishram, A. Malik, K. Narang, S. Vinayak, and R. Singh, "Cumulative dose γ-irradiation effects on material properties of AlGaN/GaN hetero-structures and electrical properties of HEMT devices," *Semicond. Sci. Technol.*, vol. 34, no. 6, 2019, Art. no. 065024, doi: 10.1088/1361-6641/ab11a0.

[32] C. Sharma, N. Modolo, T. L. Wu, M. Meneghini, G. Meneghesso, E. Zanoni, A. K. Visvkarma, S. Vinayak, and R. Singh, "Understanding γ-ray induced instability in AlGaN/GaN HEMTs using a physics-based compact model," in *IEEE Trans. Electron Devices*, vol. 67, no. 3, pp. 1126–1131, Mar. 2020, doi: 10.1109/TED.2020.2965555.

[33] T. J. Anderson, A. D. Koehler, M. J. Tadjer, K. D. Hobart, P. Specht, M. Porter, T. R. Weatherford, B. Weaver, J. K. Hite, and F. J. Kub, "Reliability of GaN HEMTs: Electrical and radiation-induced failure mechanism," in *ECS Trans.*, vol. 58, no. 4, pp. 221–225, 2013, doi: 10.1149/05804.0221ecst.

[34] A. S. Youssouf, M. H. Habaebi, and N. F. Hasbullah, "The radiation effect on low noise amplifier implemented in the space-aerial-terrestrial integrated 5G networks," *IEEE Access*, vol. 9, pp. 46641–46651, 2021, doi: 10.1109/ACCESS.2021.3065497.

[35] S. Raut, K. Sehra, M. Mishra, D. S. Rawal, M. Gupta, and M. Saxena, "Proton irradiation effects on buffer-free gallium nitride on silicon carbide high electron mobility transistor-based radio frequency power amplifier," *Semicond. Sci. Technol.*, vol. 36, no. 4, 2021, Art. no. 045019, doi: 10.1088/1361-6641/abe2df.

[36] V. K. Pandey, C. Ming Tan, and S. Sharma, "Design of GaN based comparator circuit for radiation detectors," in *Proc. 17th India Council Int. Conf. (INDICON)*, 2021, pp. 1–6, doi: 10.1109/INDICON49873.2020.9342196.

[37] M. Hofstetter, J. Howgate, I. D. Sharp, M. Stutzmann, and S. Thalhammer, "Development and evaluation of gallium nitride-based thin films for X-ray dosimetry," *Phys. Med. Biol.*, vol. 56, no. 11, pp. 3215–3231, 2011, doi: 10.1088/0031-9155/56/11/004.

[38] J. D. Howgate, M. Hofstetter, S. J. Schoell, M. Schmid, S. Schäfer, I. Zizak, V. Hable, C. Greubel, G. Dollinger, S. Thalhammer, M. Stutzmann, and I. D. Sharp, "Ultrahigh gain AlGaN/GaN high energy radiation detectors," *Phys. Status Solidi*, vol. 209, no. 8, pp. 1562–15667, 2012, doi: 10.1002/pssa.201228097.

[39] K. Sehra, V. Kumari, M. Gupta, M. Mishra, D. S. Rawal, and M. Saxena, "Degradation mechanisms in a proton irradiated HEMT with 3DEG conduction and 3DHG as a back barrier," in *Proc. IEEE Int. Conf. Nanotechnol. (NANO)*, Oct. 2021, pp. 173–176, doi: 10.1109/NANO51122.2021.9514295.

[40] A. Sandupatla, S. Arulkumaran, N. G. Ing, S. Nitta, J. Kennedy, and H. Amani, "Vertical GaN-on-GaN Schottky diodes as α-particle radiation sensors," *Micromachines*, vol. 11, no. 5, pp. 1–21, 2020, doi: 10.3390/mi11050519.

[41] *Silvaco Victory TCAD Tool Ver. 1.14.1.R and Silvaco Victory Process Tool Ver. 7.30.4.R*. Accessed: Jul. 20, 2021. [Online]. Available: https://www.silvaco.com

[42] K. Sehra, V. Kumari, M. Gupta, M. Mishra, D. S. Rawal, and M. Saxena, "Impact of heavy ion particle strike induced single event transients on conventional and π-Gate AlGaN/GaN HEMTs," in *Semicond. Sci. Technol.*, vol. 36, no. 3, 2021, Art. no. 035009, doi: 10.1088/1361-6641/abdba3.

[43] P. V. Raja, J. C. Nallatamby, N. DasGupta, and A. DasGupta, "Trapping Effects on AlGaN/GaN HEMT Characteristics," *Solid State Electron.*, vol. 176, Oct. 2021, Art. no. 107929, doi: 10.1016/j.sse.2020.107929.

[44] N. K. Subramani, J. Couvidat, A. A. Hajjar, J. C. Nallatamby, D. Floriot, and M. Prigent, "Low-frequency noise characterization in GaN HEMTs: Investigation of deep levels and their physical properties," *IEEE Electron Device Lett.*, vol. 38, no. 8, pp. 1109–1112, Feb. 2017, doi: 10.1109/LED.2017.2717539.

[45] S. Yang, S. Huang, J. Wei, Z. Zheng, Y. Wang, J. He, and K. J. Chen, "Identification of trap states in p-GaN layer of a p-GaN/AlGaN/GaN power HEMT structure by deep-level transient spectroscopy," in *IEEE Electron Device Lett.*, vol. 41, no. 5, pp. 685–688, Oct. 2020, doi: 10.1109/LED.2020.2980150.

[46] O. Aktas, A. Kuliev, V. Kumar, R. Schwindt, S. Toshkov, D. Costescu, J. Stubbins, and I. Adesida, "60Co gamma radiation effects on DC, RF, and pulsed I–V characteristics of AlGaN/GaN HEMTs," *Solid-State Electron.*, vol. 48, no. 3, pp. 471–475, Mar. 2004, doi: 10.1016/j.sse.2003.08.003.

[47] A. M. Kurakiun, S. A. Vitusevich, S. V. Danylyuk, H. Hardtdegen, N. Klein, Z. Bougrioua, B. A. Danilchenko, R. V. Konakova, and A. E. Belyaev, "Mechanism of mobility increase of the two-dimensional electron gas in AlGaN/GaN heterostructures under small dose gamma irradiation," in *J. Appl. Phys.*, vol. 103, no. 8, pp. 1–6, 2008, doi: 10.1063/1.2903144.
[48] S. A. Vitusevich, A. M. Kurakin, R. V. Konakova, A. E. Belyaev, and N. Klein, "Improvement of interface properties of AlGaN/GaN heterostructures under gamma-radiation," *Appl. Surf. Sci.*, vol. 255, no. 3, pp. 784–786, Nov. 2008, doi: 10.1016/j.apsusc.2008.07.029.
[49] A. Yadav, E. Flitsiyan, L. Chernyak, F. Ren, S. J. Pearton, J. W. Johnson, and I. Lubomirsky, "Impact of low dose gamma irradiation on electronic carrier transport in AlGaN/GaN high electron mobility transistors," *MRS Proc.*, vol. 1792, pp. 1–4, Jan. 2015, doi: 10.1557/opl.2015.511.
[50] J. Lee, A. Yadav, M. Antia, V. Zaffino, E. Flitsiyan, L. Chernyak, J. Salzman, B. Meyler, S. Ahn, F. Ren, and S. J. Pearton, "Low dose 60Co gamma-irradiation effects on electronic carrier transport and DC characteristics of AlGaN/GaN high-electron-mobility transistors," *Radiat. Effects Defects Solids*, vol. 172, nos. 3–4, pp. 250–256, Apr. 2017, doi: 10.1080/10420150.2017.1300903.
[51] K. William, Y. Xi, and D. Naus, "A review of the effects of radiation on microstructure and properties of concretes used in nuclear power plants," *United States Nucl. Regulatory Commission*, vol. 263, pp. 1–131, Oct. 2013. Accessed: Jul. 20, 2021. [Online]. Available: https://www.nrc.gov/docs/ML1332/ML13325B077.pdf
[52] C. Sharma, A. K. Visvkarma, R. Laishram, A. Kumar, D. S. Rawal, S. Vinayak, and R. Singh, "Effect of γ-ray irradiation on Schottky and ohmic contacts on AlGaN/GaN hetero-structures," in *Microelectron. Rel.*, vol. 105, May 2020, Art. no. 113565, doi: 10.1016/j.microrel.2019.113565.
[53] X. Zheng, S. Feng, C. Peng, G. Lin, L. Bai, X. Li, Y. Yang, S. Pan, Z. Hu, X. Li, and Y. Zhang, "Evidence of GaN HEMT Schottky gate degradation after gamma irradiation," *IEEE Trans. Electron Devices*, vol. 66, no. 9, pp. 3784–3788, Sep. 2019, doi: 10.1109/TED.2019.2928560.
[54] P. J. Martánez, E. Maset, P. M.-. Holgado, Y. Morilla, D. Gilabert, and E. S. Kilders, "Impact of gamma radiation on dynamic RDSON characteristics in AlGaN/GaN power HEMTs," *Material*, vol. 12, no. 7, pp. 1–15, 2019, doi: 10.3390/ma12172760.
[55] Y. Qi, D. Wang, J. Zhou, K. Zhang, Y. Kong, S. Wu, and T. Chen, "Effect of X-ray irradiation on threshold voltage of AlGaN/GaN HEMTs with p-GaN and MIS gates," *Nanotechnol. Precis. Eng.*, vol. 3, no. 4, pp. 241–243, Dec. 2020, doi: 10.1016/j.npe.2020.11.001.
[56] N. Venkatesan, G. Silva-Oelker, and P. Fay, "Graded-channel GaN-based HEMTs for high linearity amplifiers at millimeter-wave," in *Proc. IEEE BiCMOS Compound Semiconductor Integr. Circuits Technol. Symp. (BCICTS)*, Feb. 2019, pp. 1–4, doi: 10.1109/BCICTS45179.2019.8972753.
[57] A. Ramu, K. Ban, D. Kimpton, S. Wilson, and R. Bayruns, "Parabolic grading of a PHEMT channel composition for ultra-high and broad OIP3 peak," in *Silvaco's Simul. Standard*, vol. 31, no. 2, pp. 1–5, 2021. Accessed: Jul. 20, 2021. [Online]. Available: https://silvaco.com/simulation-standard/parabolic-grading-of-a-phemt-channel-composition-for-ultra-high-and-broad-oip3-peak/
[58] Y. Song, T. Kujofsa, and J. E. Ayers, "Bi-parabolic graded buffer layers for metamorphic devices," *ECS Trans.*, vol. 80, no. 10, pp. 973–980, Oct. 2017, doi: 10.1149/08010.0973ecst.
[59] T. Kujofsa, M. Cai, X. Chen, T. Md Islam, and J. E. Ayers, "Optimization of graded buffer layers for metamorphic semiconductor devices," *Int. J. High Speed Electron. Syst.*, vol. 27, Feb. 2018, Art. no. 03n04, doi: 10.1142/S0129156418400232.
[60] H. Zhang, C. Huang, K. Song, H. Yu, C. Xing, D. Wang, Z. Liu, and H. Sun, "Compositionally graded III-nitride alloys: Building blocks for efficient ultraviolet optoelectronics and power electronics," *Rep. Prog. Phys.*, vol. 84, no. 4, pp. 1–29, 2021, doi: 10.1088/1361-6633/abde93.
[61] R. L. Pease, R. D. Schrimpf, and D. M. Fleetwood, "ELDRS in bipolar linear circuits: A review," in *Proc. Eur. Conf. Radiat. Effects Compon. Syst.*, 2008, pp. 18–32, doi: 10.1109/RADECS.2008.5782678.
[62] N. L. Rowsey, M. E. Law, R. D. Schrimpf, D. M. Fleetwood, B. R. Tuttle, and S. T. Pantelides, "A quantitative model for ELDRS and H_2 degradation effects in irradiated oxides based on first principles calculations," *IEEE Trans. Nucl. Sci.*, vol. 58, no. 6, pp. 2937–2944, May 2011, doi: 10.1109/TNS.2011.2169458.
[63] D. M. Fleetwood, "Total ionizing dose effects in MOS and low-dose-rate-sensitive linear-bipolar devices," *IEEE Trans. Nucl. Sci.*, vol. 60, no. 3, pp. 1706–1730, Jun. 2013, doi: 10.1109/TNS.2013.2259260.
[64] D. M. Fleetwood, "Physical mechanisms contributing to enhanced bipolar gain degradation at low dose rates," *IEEE Trans. Nucl. Sci.*, vol. 41, no. 6, pp. 1871–1883, Dec. 1994, doi: 10.1109/23.340519.
[65] D. M. Fleetwood, L. C. Riewe, J. R. Schwank, S. C. Witczak, and R. D. Schrimpf, "Radiation effects at low electric fields in thermal, SIMOX, and bipolar-base oxides," *IEEE Trans. Nucl. Sci.*, vol. 43, no. 6, pp. 2537–2546, Aug. 1996, doi: 10.1109/23.556834.
[66] J. E. Turner, *Atoms, Radiation, and Radiation Protection*. Hoboken, NJ, USA: Wiley, 2017, pp. 361–398.

KHUSHWANT SEHRA (Graduate Student Member, IEEE) received the B.Tech. degree in electronics from the University of Delhi, New Delhi, India, in 2017, and the M.Tech. degree in electronics and communication engineering from the University School of Information, Communication and Technology, Guru Gobind Singh Indraprastha University, New Delhi, in 2019. He is currently working as a Research Scholar with the Department of Electronic Science, University of Delhi. His research interests include modeling, simulation, and fabrication of GaN-based HEMT devices. He has also worked on image processing, including digital image watermarking and development of facial recognition systems for uncontrolled environments.

VANDANA KUMARI (Member, IEEE) received the B.Sc. (General), M.Sc., and Ph.D. degrees from the University of Delhi, Delhi, India, in 2006, 2009, and 2014, respectively. Currently, she is an Assistant Professor with the Maharaja Agrasen College, University of Delhi. She has authored more than 62 papers in international journals and conferences. Her research interests include modeling and simulation of unconventional MOSFET/HEMT architectures.

POONAM KASTURI (Member, IEEE) was born in Punjab, India, in March 1971. She received the B.Sc. (Hons.), M.Sc., and Ph.D. degrees in electronics from the University of Delhi, New Delhi, in 1992, 1994, and 2008, respectively. She submitted her doctoral thesis on "Two Dimensional Physics Based Analytical Modeling and Simulation of Silicon-on-Nothing (SON) MOSFET" with the Semiconductor Device Research Laboratory, Department of Electronic Science, University of Delhi. In 1995, she joined the Deen Dayal Upadhayaya College, University of Delhi, as a Lecturer. She is currently an Associate Professor with the Department of Electronics, University of Delhi. She has authored seven research papers in international journals and conferences. Her research interests include microelectronics and verilog.

MRIDULA GUPTA (Senior Member, IEEE) received the Ph.D. degree in optoelectronics from the University of Delhi, India, in 1998. Since 1989, she has been with the Department of Electronic Science, University of Delhi South Campus, where she is currently a Professor. She has authored or coauthored more than 390 publications in international and national journals and conference proceedings. Her current research interests include modeling and simulation of MOSFETs, MESFETs, and HEMTs, for microwave applications and TFET for biosensing application. She is a fellow of IETE and the Chair Person of IEEE EDS Delhi Chapter.

MEENA MISHRA (Member, IEEE) received the B.Sc. and M.Sc. degrees in electronics from Delhi University, in 1986 and 1988, respectively, and the Ph.D. degree in electronics from Jamia Millia Islamia University, New Delhi, in 2006. She has been a Scientist with the Solid State Physics Laboratory, since 1989. She was involved in designing of high frequency GaAs-based digital integrated circuits. She is currently working as a Scientist G with the Solid State Physics Laboratory, Defence Research and Development Organization, New Delhi, where she is involved in the development of RF GaN HEMT Technology. She is also involved in GaN microwave FET and GaAs MMlC research and development projects.

DIPENDRA SINGH RAWAL (Member, IEEE) received the M.Sc. degree in physics and the M.Tech. degree in electronics and communication engineering from IIT Roorkee, Roorkee, India, in 1988 and 1990, respectively, and the Ph.D. degree in physics from IIT Delhi, New Delhi, India, in 2012. He is currently working as a Scientist G with the Solid State Physics Laboratory, Defence Research and Development Organization, New Delhi, where he is involved in the development of GaN high electron mobility transistor-based monolithic microwave integrated circuit technology. He has published more than 60 research papers in various international journals and conferences.

MANOJ SAXENA (Senior Member, IEEE) received the M.Sc. and Ph.D. degrees in electronics from the University of Delhi, New Delhi, in 2000 and 2006, respectively. He is currently an Associate Professor with the Department of Electronics, Deen Dayal Upadhyaya College, University of Delhi. He has authored or coauthored 300 technical papers in international journals and conference proceedings (including 81 papers in IEEE TRANSACTIONS ON ELECTRON DEVICES, IEEE TRANSACTIONS ON DEVICE AND MATERIALS RELIABILITY, IEEE TRANSACTIONS ON NANOTECHNOLOGY, IEEE ELECTRON DEVICE LETTERS, and IEEE conference proceedings) and has delivered 30 EDS Distinguished Lecture talks in past three years. He received ''Highly Valued Volunteer for 2011–2012 EDS Chapters in South Asia, IEEE Region 10'' and has reviewed extensively IEEE journals and conferences. He is a fellow of IETE, India, and Optical Society of India. He is a member of Institute of Physics, U.K.; IET, U.K.; and The National Academy of Sciences India (NASI). He is currently an IEEE EDS Board of Governor Member and an Associate Editor-in-Chief of IEEE EDS Newsletter—Region 10 South Asia (2016) and was the Vice Chair of the IEEE EDS SRC Region 10 (2015–2017).